Experimental Neurology 311 (2019) 88–105

Contents lists available at ScienceDirect

Experimental Neurology

journal homepage: www.elsevier.com/locate/yexnr

Research paper

Early intrathecal infusion of everolimus restores cognitive function and mood in a murine model of Alzheimer's disease

Tommaso Cassano[a,*], Alessandro Magini[b], Stefano Giovagnoli[c], Alice Polchi[b], Silvio Calcagnini[d], Lorenzo Pace[a], Michele Angelo Lavecchia[d], Caterina Scuderi[d], Maria Rosanna Bronzuoli[d], Loredana Ruggeri[e], Maria Pia Gentileschi[f], Adele Romano[d], Silvana Gaetani[d], Federico De Marco[f], Carla Emiliani[b], Diego Dolcetta[f,**]

[a] Department of Clinical and Experimental Medicine, Medical School, University of Foggia, 71100 Foggia, Italy
[b] Department of Chemistry, Biology and Biotechnology, University of Perugia, 06126 Perugia, Italy
[c] Department of Pharmaceutical Sciences, University of Perugia, 06123 Perugia, Italy
[d] Department of Physiology and Pharmacology "V. Erspamer", Sapienza University of Rome, 00185 Rome, Italy
[e] Division of Hematology and Clinical Immunology and Bone Marrow Transplant Program, Department of Medicine, University of Perugia, 06132 Perugia, Italy
[f] UOSD SAFU, RiDAIT Dept, The Regina Elena National Cancer Institute, 00144 Rome, Italy

ARTICLE INFO

Keywords:
Intrathecal administration
Everolimus
Mammalian target of rapamycin
Alzheimer's disease
Depression
Learning and memory
3 × Tg-AD mice

ABSTRACT

The discovery that mammalian target of rapamycin (mTOR) inhibition increases lifespan in mice and restores/delays many aging phenotypes has led to the identification of a novel potential therapeutic target for the treatment of Alzheimer's disease (AD). Among mTOR inhibitors, everolimus, which has been developed to improve the pharmacokinetic characteristics of rapamycin, has been extensively profiled in preclinical and clinical studies as anticancer and immunosuppressive agent, but no information is available about its potential effects on neurodegenerative disorders. Using a reliable mouse model of AD (3 × Tg-AD mice), we explored whether short-term treatment with everolimus injected directly into the brain by osmotic pumps was able to modify AD-like pathology with low impact on peripheral organs.

We first established in non-transgenic mice the stability of everolimus at 37 °C in comparison with rapamycin and, then, evaluated its pharmacokinetics and pharmacodynamics profiles through either a single peripheral (i.p.) or central (i.c.v.) route of administration. Finally, 6-month-old (symptomatic phase) 3 × Tg-AD mice were treated with continuous infusion of either vehicle or everolimus (0.167 μg/μl/day, i.c.v.) using the osmotic pumps. Four weeks after the beginning of infusion, we tested our hypothesis following an integrated approach, including behavioral (tests for cognitive and depressive-like alterations), biochemical and immunohistochemical analyses.

Everolimus (i) showed higher stability than rapamycin at 37 °C, (ii) poorly crossed the blood-brain barrier after i.p. injection, (iii) was slowly metabolized in the brain due to a longer $t_{1/2}$ in the brain compared to blood, and (iv) was more effective in the CNS when administered centrally compared to a peripheral route. Moreover, the everolimus-induced mTOR inhibition reduced human APP/Aβ and human tau levels and improved cognitive function and depressive-like phenotype in the 3 × Tg-AD mice.

The intrathecal infusion of everolimus may be effective to treat early stages of AD-pathology through a short and cyclic administration regimen, with short-term outcomes and a low impact on peripheral organs.

1. Introduction

Alzheimer's disease (AD) is an age-related neurodegenerative disorder clinically characterized by a progressive deterioration of cognitive function. AD is defined pathologically by the presence of amyloid plaques, composed of aggregated amyloid β-peptides (Aβ), and neurofibrillary tangles (NFTs), composed of hyperphosphorylated and aggregated tau protein. Despite recent advances in treatment strategies, AD remains incurable and new therapeutic targets are needed.

The mammalian target of rapamycin (mTOR) signaling pathway has

* Correspondence to: T. Cassano, Department of Clinical and Experimental Medicine, University of Foggia, Viale Luigi Pinto 1, 71100 Foggia, Italy.
** Correspondence to: D. Dolcetta, UOSD SAFU, RiDAIT Department, The Regina Elena National Cancer Institute, via Elio Chianesi 53, 00144 Rome, Italy.
E-mail addresses: tommaso.cassano@unifg.it (T. Cassano), diego.dolcetta@gmail.com (D. Dolcetta).

https://doi.org/10.1016/j.expneurol.2018.09.011
Received 23 March 2018; Received in revised form 13 August 2018; Accepted 17 September 2018
Available online 20 September 2018
0014-4886/

received much attention for its role in the aging process (Powers et al., 2006; Vellai et al., 2003). In fact, the inhibition of mTOR leads to a number of downstream events including the inhibition of cellular proliferation and the stimulation of autophagy, an intracellular degradation pathway essential for cellular and energy homoeostasis (Harrison et al., 2009; Powers et al., 2006; Vellai et al., 2003). Since neurodegeneration-associated aggregation-prone proteins are predominantly degraded by autophagy (Kim et al., 2011), emerging evidence indicates that compromised autophagy can lead to the accumulation of mutant proteins and cellular toxicity. Enhancing this process exerts beneficial effects in a wide range of transgenic disease models (Harrison et al., 2009; Majumder et al., 2011, 2012).

In particular, genetic and pharmacological reduction of mTOR activity has been shown to significantly increase the lifespan in different organisms including yeast, Drosophila and mammals (Harrison et al., 2009; Majumder et al., 2012; Powers et al., 2006; Vellai et al., 2003). Moreover, mTOR signaling was reported to be up-regulated in Down's syndrome patients and in selected neurons of AD brains that are predicted to develop tau pathology suggesting that chronic high levels of mTOR signaling may exert detrimental effects in both Down's syndrome and AD brains (An et al., 2003; Iyer et al., 2014). Furthermore, the neuropathological alterations and learning and memory deficits in animal models of AD and tuberous sclerosis were associated with an increase in mTOR signaling (Caccamo et al., 2010, 2011; Ehninger et al., 2008; Magini et al., 2017).

Rapamycin, an immune-modulator approved by the U.S. Food and Drug Administration (FDA) for clinical use as an immunosuppressant, rescues cognitive deficits and ameliorates Aβ and tau pathology by increasing autophagy (Caccamo et al., 2010). Inhibition of mTOR signaling also has beneficial effects in murine models of Apolipoprotein E4-related and Down's syndrome-related AD (Andrade-Talavera et al., 2015; Lin et al., 2017).

In all these studies, the drug was chronically administered orally for 2 to 6 months (Andrade-Talavera et al., 2015; Caccamo et al., 2010; Lin et al., 2017). However, more recent studies have demonstrated that long-term treatment with mTOR inhibitors resulted in mTOR complex 1 (mTORC1) resistance and the development of autophagy inhibition (Kurdi et al., 2016), due to an uncoupling of the mTORC1 substrate, the unc-51-like autophagy-activating kinase 1 (ULK1). This suggests that the long-term use of mTOR inhibitors as a treatment for AD may have limited value. ULK1 is the main effector by which mTORC1 is able to initiate autophagy (Kim et al., 2011). Moreover, the chronic administration of rapamycin is associated with detrimental effects on metabolism, including hyperglycemia, hyperlipidemia, and insulin resistance in a murine model of nutrition-dependent type-2 diabetes (Fraenkel et al., 2008), and similar metabolic changes have been shown in patients treated with rapamycin (Stallone et al., 2009).

One potential new approach to administer novel experimental therapies with the beneficial effects of mTOR inhibition but fewer systemic side effects is to administer local intracerebroventricular (i.c.v.) infusion of the mTOR inhibitor directly into the brain. Intracerebroventricular access is routinely used in any event that might impede normal cerebrospinal fluid outflow (Fried et al., 2016). The same route can also operate in the opposite direction and serve as an efficient route for drug delivery into the ventricular space (Peyrl et al., 2014). This route of administration is currently exploited in case of meningitis that are sensitive to antibiotics that do not readily cross the blood-brain barrier (Arnell et al., 2007), or in primary brain lymphoma cases that are sensitive to high doses of anticancer drugs, which are only achievable locally without causing intolerable side effects (Korfel and Schlegel, 2013).

Previous studies have demonstrated that i.c.v. infusion is reliable in humans (Arnell et al., 2007; Korfel and Schlegel, 2013; Peyrl et al., 2014), therefore in this study we examined the efficacy of administering everolimus, a synthetic analogue of rapamycin into the cerebroventricular space of a triple transgenic model of AD (3 × Tg-AD). These mice develop age-dependent and region-specific Aβ and tau aggregations that closely mimic the disease progression seen in humans (Bellanti et al., 2017; Cassano et al., 2011, 2012; Oddo et al., 2003; Romano et al., 2014).

Although the antitumor properties of everolimus have been extensively profiled in preclinical (Mabuchi et al., 2007) and clinical studies (Motzer et al., 2008), little has been reported about its pharmacokinetics and potential effects on neurodegenerative disorders.

Therefore, we initially performed an exploratory study on non-transgenic (Non-Tg) mice and investigated the pharmacokinetic behavior of everolimus administered through different routes (i.p. *vs* intrathecal). We, then, investigated the effects of a short-term intrathecal infusion of everolimus on cognitive and non-cognitive components of behavior, as well as the disease-modifying potential (*i.e.*, ability to reduce the brain levels of Aβ and hyperphosphorylated tau) in young/adult 3 × Tg-AD mice.

Briefly, our results suggest that intrathecal everolimus treatment enhances cognitive function and exerts antidepressant-like effects in young/adult 3 × Tg-AD mice. In addition, our data demonstrate that everolimus reduces both human APP/Aβ and human tau levels in 3 × Tg-AD mice.

2. Material and methods

2.1. Experimental chemicals and reagents

Everolimus was purchased from Selleckchem (> 99%, cat. N. S1120, Munich, Germany), rapamycin from Ningbo Heyreal Import & Export Co., Ltd. (Zhejiang, China), carboxymethylcellulose sodium salt and polysorbate-80 were from Sigma-Aldrich (> 99%, Milan, Italy). HPLC-grade methanol, ammonium formate and acetonitrile were from J. T. Baker (Milan, Italy), formic acid was from Sigma-Aldrich (> 98%, Milan, Italy). Zinc sulfate was from Carlo Erba (> 99%, Milan, Italy). HPLC-grade water was obtained from inverse-osmosis MilliQ system. The osmotic pumps (model 1002) were purchased from Alzet (Cupertino, CA, USA).

2.2. Evaluation of everolimus and rapamycin stability in artificial cerebrospinal fluid

In order to evaluate the stability of everolimus during its delivery by osmotic pumps in animal models, everolimus and its natural analogue rapamycin were dissolved at a concentration of 10 μg/ml in a vehicle solution consisting of 10% (v/v) DMSO in artificial cerebrospinal fluid (aCSF) containing, in mM, NaCl 145, KCl 2.7, $MgCl_2$ 1, $CaCl_2$ 2.4, and Na_2HPO_4 2, buffered at pH 7.4. Samples were then incubated at 37 °C and aliquots were withdrawn at established time intervals and submitted to HPLC-UV analysis. The concentrations of everolimus and rapamycin were then measured over time and were expressed as a percentage of the initial value, which was set to 100%.

2.3. Everolimus quantification by HPLC-UV method

The UV method was based on previously published work (Giovagnoli et al., 2015). The instrument used was a Portlab STAYER HPLC system equipped with UV detection, a parallel pump and Triathlon autosampler (Portlab, Rome, Italy). The conditions employed were the following: isocratic mode with acetonitrile:water (60:40, v/v) eluted at 0.9 ml/min and a Zorbax sb-300 C18 column (Agilent, Milan, Italy) equilibrated at 60 °C. UV detection was performed at 278 nm and calibration was performed between 25 and 200 ng/ml (r^2 = 0.99957).

2.4. Evaluation of everolimus and rapamycin stability in cells

Everolimus and rapamycin stability were determined by evaluating cell proliferation after drug treatment (Polchi et al., 2016). Both

everolimus and rapamycin were resuspended in DMSO at concentration of 10 mg/ml and were diluted to 1 μM in vehicle solution and were used fresh or maintained in incubator at 37 °C for 7 and 14 days.

Their pharmacological activity was tested *in vitro* on SH-SY5Y, a neuroblastoma cell line obtained from American Type Culture Collection (ATCC, Manassas, VA, USA). Cells were grown in Dulbecco's modified Eagle's medium (DMEM) (Gibco) supplemented with 10% (v/v) FBS (Gibco), 1% (v/v) penicillin/streptomycin (Gibco), 2 mM L-glutamine (Gibco) in a humidified incubator at 37 °C and 5% CO_2. SH-SY5Y cells were treated with 2 nM rapamycin and 40 nM everolimus, and cell proliferation was estimated by 3-[4,5-dimethylthiazol-2-yl]-2,5- diphenyltetrazolium bromide (MTT, Sigma Aldrich) test, as previously reported (Polchi et al., 2016). As a control, cells were treated with the same concentration of DMSO used for drug treatment. Briefly, SH-SY5Y cells were seeded in a 96-well plate at the concentration of 5×10^4 cells/cm^2 and maintained in medium (100 μl). Each experiment was carried out on six replicates and the assays were performed at 0, 24 and 48 h of drug treatment. Results were reported as mean ± SEM of three independent experiments (group). Cells were mixed with 0.5 mg/ml MTT and maintained for 4 h in a humidified incubator. Successively, 100 μl of 10% SDS and 0.01 N HCl solution were added to the well. Next day, spectrophotometric readings were performed on Beckman Coulter DTX 880 Multimode Detector (Beckman Coulter Inc., Brea, CA, USA) using a 570 nm line and 650 nm reference.

2.5. Animals

6-month-old 3 × Tg-AD male mice and their wild type male littermates (Non-Tg) were used in this study. The 3 × Tg-AD mice harbor APP_{swe}, $PS1_{M146V}$, and tau_{P301L} transgenes and the background strain is C57BL6/129SvJ hybrid (Oddo et al., 2003). Genotypes were confirmed by polymerase chain reaction after tail biopsies (Cassano et al., 2011, 2012; Oddo et al., 2003). Animals were maintained under standard conditions (12:12 light–dark cycle; temperature at 22 °C; 50–60% relative humidity; *ad libitum* access to food and water). All the experiments were performed in strict compliance with the Italian National Laws (DL 116/92) and the European Communities Council Directives (86/609/EEC) (IACUC protocol number 443/13). All efforts were made to minimize the number of animals used and their suffering.

2.6. Pharmacokinetics of everolimus and mTOR inhibition

The aim of this first *in vivo* experiment was the comparative pharmacokinetic analysis of everolimus after either a single intraperitoneal (i.p.) or intracerebroventricular (i.c.v.) administration in Non-Tg mice. After both routes of administration, pharmacokinetic parameters of everolimus in the whole blood and cerebral tissues were determined, as well as the degree of mTOR inhibition in the brain.

To this purpose, Non-Tg mice were randomly divided into two groups (12 mice/group) to receive either i.p. or i.c.v. administration of everolimus, respectively.

For the i.p. administration, everolimus was diluted from 10% (*v*/v) DMSO stock into saline and injected at a dose of 5 mg/kg in a volume of 10 ml/kg body weight. The selection of the dose was based on consideration of everolimus blood concentrations in previous studies (Muller et al., 2008; O'Reilly et al., 2009).

As far as the i.c.v. administration, everolimus was diluted from 10% (v/v) DMSO stock into aCSF and injected into the right lateral ventricle at a dose of 0.167 μg/μl in a volume of 6 μl through a 33G needle injector attached to a 10 μl Hamilton syringe. This dose was chosen based on previous experiments conducted treating mice with decreasing dosages of the drug (data not shown). Before i.c.v. administration, mice were anesthetized by i.p. injection of ketamine hydrochloride (1 mg/10 g) and xylazine (0.1 mg/10 g) and placed in a stereotactic apparatus with a mouse adaptor. The coordinates from the bregma were 0.5 mm anterior-posterior, 1.1 mm medio-lateral, and 2.5 mm dorso-ventral to the skull (Franklin and Paxinos, 1997). Injections occurred over 5 min, and the cannula was left in place for an additional 5 min to allow diffusion. Incisions were closed with instant dental cement. 1, 3 and 5 h after either i.p and i.c.v. administration, Non-Tg mice were sacrificed and 0.5 ml of the trunk blood was collected in ice-cold tubes containing 50 μl of K_2-EDTA (20%, w/v), whereas brains were rapidly excised, divided into two hemispheres and then immediately frozen in dry ice. The left hemisphere was used to detect mTOR inhibition by immunoblotting analysis, whereas the right hemisphere and the whole blood samples were used for the detection of everolimus levels.

Blood samples were preliminary exposed to intensive sonication for 10 min to induce haemolysis, and then frozen at −70 °C until everolimus detection by the HPLC method (Giovagnoli et al., 2015).

2.7. Osmotic pump implantation and intracerebroventricular everolimus administration

We next tested the effects of everolimus when delivered continuously into the brain by an osmotic pump (Alzet 1002, 0.25 μl per hour, 14 days) for 2 weeks (see the timeline of the experiments in Fig. 3). Osmotic pumps were loaded with either vehicle or everolimus solution delivered at 0.167 μg/μl/day.

Before implantation, Alzet pumps (100 μl) were filled with everolimus and kept in 0.9% saline at 37 °C overnight according to the manufacturer's protocol. Mice were anesthetized with an i.p. injection of ketamine hydrochloride (1 mg/10 g) and xylazine (0.1 mg/10 g). After being shaved on the head and back, a cannula was inserted into the right lateral ventricle using stereotaxic coordinates, as previously reported. The cannula was secured to the skull by using instant dental cement and was connected *via* polyethylene tubing to an osmotic pump placed subcutaneously on the back. After surgery, the mice were kept on a warming plate until recovery from anaesthesia, and then housed individually.

A first cohort (n = 18 mice) of Non-Tg mice was infused with either everolimus or vehicle and sacrificed at 3, 5 and 10 days from the beginning of the infusion. At each time-point, brain and liver were rapidly excised and immediately frozen on dry ice for further evaluation of mTOR inhibition. In particular, the expression of total and phosphorylated p70 ribosomal S6 kinase (p70S6K) protein, a downstream effector of the mTORC1 signaling pathway, was detected in each sample by immunoblotting analysis. Moreover, at 10 days from the beginning of the infusion, spleen and femur were also excised and were used to evaluate the effect of everolimus-infusion on the cells from mouse bone marrow and spleen. In particular, spleen cells obtained by mechanical shredding were suspended in phosphate-buffered saline (PBS) and counted. Bone marrow was flushed out from femur using a syringe and an insulin needle, put in suspension and counted.

A second cohort (n = 10 mice, with 5 mice per group) of 3 × Tg-AD mice was infused with either everolimus or vehicle and sacrificed 4 weeks later when mice reached 7 months of age. Their brains were extracted and cut in half sagittally. One-half of the brain was freshly dissected to isolate the hippocampus and the frontal cortex, which are the brain regions mostly affected by the neuropathological hallmarks of AD. Both of them were frozen in dry ice and, then, the effect of everolimus on the amyloid precursor protein (APP) processing and tau phosphorylation was evaluated by immunoblotting analysis.

For the immunohistochemical analysis of Aβ and human tau, the other half of the brain was dropped-fixed in 4% paraformaldehyde in PBS for 48 h and then transferred in a 25% sucrose solution in PBS overnight. After removal of excess sucrose, brains were frozen in 2-methylbutane (−50 °C) until slicing.

A third cohort (n = 40 mice, with 10 mice per group) of 3 × Tg-AD and Non-Tg mice was infused with either everolimus or vehicle and left undisturbed in their home cages for 4 weeks and, then, subjected to behavioral testing when the mice reached 7 months of age.

2.8. Behavioral testing

Tests were conducted on the third cohort of 7-month-old 3 × Tg-AD and Non-Tg mice. We used a serial behavioral testing procedure that has been validated and compared with single testing procedures in our laboratory, and by other investigators (Bambico et al., 2010; Giustino et al., 1999; Romano et al., 2014; Scuderi et al., 2018; Barone et al., 2018).

The novel object recognition test (NORT), the inhibitory passive avoidance (IA) and the Morris water maze (MWM) test were used to explore the cognitive behaviors, whereas the sucrose preference test (SPT), the tail suspension test (TST) and the forced swim test (FST) for antidepressant/depression-like coping behaviors. The sequence in which the experimental procedures were administered to the animals is described in Fig. 3, starting with those considered to be least stressful. The minimum interval between two consecutive procedures was 2 days. It is worth noting that repeated behavioral testing may alter mouse's behavioral responses, although it has been shown that these effects can be limited, as in the case of the water maze (Chen et al., 2000).

All tests were performed between 8:00 a.m. and 3:00 p.m., in a dimly lit environment. On the day of testing, the mice were acclimated for about 60 min in the behavioral room before the procedures were initiated. The apparatus was cleaned with 70% alcohol and water after each run. The behaviors were recorded with infrared lighting-sensitive CCD cameras, stored, and analysed as MPEG files. Behaviors were evaluated by both direct observation and analysis of videotape-recorded images by an observer unaware of the animals' genotype and treatment. Experimental subjects were weighed every day during the entire period of the experiment.

Novel object recognition test (NORT) – The object recognition task is based on the spontaneous tendency of rodents to explore a novel object longer than a familiar one. Each mouse was habituated to an empty Plexiglas arena (45 × 25 × 20 cm) for 3 consecutive days. On training session (T1) (day 4), mice were exposed for 5 min to two identical objects (A + A) placed at opposite ends of the arena. 30 min and 24 h later, the animals were subjected to a 5 min testing session where they were exposed to one familiar object (A) and to a novel object B (after 30 min) and object C (after 24 h). Exploration was considered as pointing the head toward an object at a distance of < 2.5 cm from the object, with its neck extended and vibrissae moving. Turning around, chewing, and sitting on the objects were not considered exploratory behaviors. The time of exploration was recorded, and an object recognition index (ORI) were calculated, such that ORI = (TN − TF)/(TN + TF), where TN and TF represent times of exploring the novel and familiar object, respectively (Giustino et al., 1999; Scuderi et al., 2018). Mice that did not explore both objects during training were discarded from further analysis. Objects used in this task were carefully selected to prevent preference or phobic behaviors. To avoid olfactory cues, the objects were thoroughly cleaned with 70% ethanol and the sawdust was stirred after each trial.

Sucrose preference test (SPT) – One of the main symptoms of depression is anhedonia, defined as the inability to experience any kind of pleasure. This function can be evaluated in rodents as a decrease in the capacity of response to reward, such as a sucrose solution (Katz, 1982). The SPT was performed as previously described (Romano et al., 2014). Briefly, the animals were isolated in small cages (22.5 cm × 14 cm × 16.7 cm). Each of them had free access to two drinking bottles, the first filled with 100 ml of tap water, while the other with a solution of sucrose to 2%. Before the test, there was a period of adaptation lasting 48 h, in order to accustom the animals to the different types of fluids. The animals were then deprived of food and liquids for 3 h. During the next 24 h, free consumption of water and 2% sucrose solution took place, in the presence of *ad libitum* food. Fluid intake was measured afterwards by weighing the drinking bottles. Sucrose preference was calculated from the amount of sucrose solution consumed, expressed as a percentage of the total amount of liquid drunk.

Inhibitory passive avoidance (IA) – In this test experimental subjects learn to avoid an environment, which provides an aversive stimulus (foot-shock). The IA was performed as previously described (Scuderi et al., 2018). Briefly, on training, mice were placed in the fear-conditioning chamber and were allowed to explore for 2 min before receiving three electric foot shocks (1 s, 0.1 mA; intershock interval, 2 min). Animals were returned to the home cage 30 s after the last foot shock. Animals were subsequently tested 24 h or 7 days after the training phase to assess their short- and long-term memory. During this phase, their behavior in the conditioning chamber was video recorded for 5 min and subsequently was analysed for freezing behavior, which was defined as the absence of all movement except for respiration.

Tail suspension test (TST) – This procedure, which is also used to assess antidepressant-like activity, involved suspending the mouse by the tail from a lever in a white box (30 × 30 × 30 cm). The test has duration of 6 min and is calculated by the immobility time (*sec*) in the last 4 min of recording. These experimental conditions were similar to those described by Romano et al. (2014). Antidepressant treatment significantly reduces the total time the mouse remains immobile.

Forced swim test (FST) – The FST examines the dynamics of transition from an active (swimming) to a passive (immobility) mode of coping in an inescapable water-filled pool. Enhancement of immobility normally ensues after exposure, a phenomenon argued to reflect learned behavioral despair (Porsolt et al., 1977) and is prevented by antidepressant treatment. The FST was performed as previously described (Bambico et al., 2010; Romano et al., 2014; Scuderi et al., 2018). Briefly, mice were placed individually into Plexiglas cylindrical bins (20 cm diameter, 50 cm high) filled with water (25–27 °C water temperature) to a depth of 20 cm. This depth did not allow the tail and hindpaws to touch the floor of the bin. The mice were then allowed to swim for 6 min. After recording, the mice were rescued using a plastic grid and caged near a heat source (lamp). The behavioral tracking system was calibrated so that a mouse was considered immobile when making only those movements necessary to keep its head above water. The total duration of activity was determined during the last 4 min.

Morris water maze (MWM) – The test was conducted in a circular tank of 1.2 m in diameter, located in a room with several extra maze cues as previously described (Scuderi et al., 2018). Briefly, mice were trained to swim to a 14-cm-diameter circular Plexiglas platform submerged 1.5 cm beneath the surface of the water and invisible to the mouse while swimming. The water temperature was kept at 25 °C throughout the duration of the testing. The platform was fixed in place, equidistant from the center of the tank and its walls. Mice were subjected to 4 training trials per day and were alternated among 4 random starting points for 5 consecutive days. Mice were allowed to find and escape onto the submerged platform. If the mice failed to find the platform within 60 s, they were manually guided to the platform and were allowed to remain on it for 10 s. After this, each mouse was placed into a holding cage under a warming lamp for 25 s until the start of the next trial. Retention of the spatial training (the probe trial) was assessed 1.5 and 24 h after the last training session and consisted of a 60-s trial without the platform. Mice were monitored by a camera mounted in the ceiling directly above the pool, and all trials were video recorded for subsequent analysis. The parameters measured during the probe trial included (1) initial latency to cross the platform location and (2) time spent in the target quadrant (Scuderi et al., 2018). Performance was monitored using the EthoVision XT version 7 video tracking software system (Noldus Information Technology Inc., Leesburg, VA).

2.9. Protein extraction and immunoblotting analysis

The frozen tissues (brain and liver) were thawed in ice-cold RIPA buffer (pH 7.4) containing 50 mM Tris-HCl (pH 7.4), 150 mM NaCl, 1% NP-40, 0.5% sodium deoxycholate, 1 mM EDTA, 0.1% SDS, supplemented with the proper protease inhibitor cocktail

(phenylmethylsulfonyl fluoride 1 mM, aprotinin 10 μg/ml, leupeptin 0.1 mM and sodium orthovanadate 1 mM, all from Sigma-Aldrich). Tissues were homogenized by sonication (UP50H, Hielscher, USA) and the resulting homogenates were centrifuged at 14,000 rpm for 15 min at 4 °C to remove cellular debris. The supernatants were extracted to determine the total protein concentration by the Bradford assay and then stored at −80 °C until use.

For western blot analyses, proteins were resolved on 12% precast polyacrylammide gels (12% Mini-PROTEAN® TGX™, BioRad, Hercules, CA, USA) under reducing conditions and were transferred to a nitrocellulose membrane. Membranes were blocked for 1 h in 5% (*w/v*) nonfat dry milk powder in Tris-buffered saline-Tween 20 0.1% (TBS-T) and incubated for 1 h with one of the following antibodies: mouse monoclonal anti-β-amyloid 1–16 (6E10) (1:1000, SIG-39320, Signet Laboratories-Covance, Emeryville, CA, USA), mouse monoclonal anti-phospho-tau AT8 and AT180 (1:1000, MN1020 and MN1040, Thermo Scientific, Waltham, MA, USA), rabbit polyclonal anti-beta-site APP cleaving enzyme 1 (BACE-1) (1:1000, Abcam plc, Cambridge, UK), rabbit polyclonal anti-Phospho-p70S6K (T389), rabbit polyclonal anti-p70S6K and rabbit polyclonal anti-β-actin (1:5000, ab8227, Abcam plc) was used as control. After being extensively washed in TBS-T, membranes were incubated for 1 h in the proper secondary horseradish peroxidase- (HRP)-conjugated antibodies goat anti-rabbit or goat anti-mouse IgG (1:5000, Jackson Immunoresearch, Europe, Suffolk, UK). Membranes were developed with a chemiluminescent HRP Substrate kit (WesternBright™ ECL, Advansta Corporation, Menlo Park, CA, USA), acquired with Chemi-Doc MP (Bio-Rad, Hercules, CA, USA) and analysed using Image Lab software version 5.2.1 (Bio-Rad, Hercules, CA, USA). Furthermore, to confirm the specificity of 6E10 for the detection of APP and for human APP/Aβ and human tau was also carried out without the primary antibody. Results were expressed as percentage of vehicle-treated animals, after being normalized with respect to β-actin.

2.10. Immunohistochemistry

Immunohistochemical staining for human APP/Aβ and human tau was performed as previously described (Barone et al., 2016; Bedse et al., 2014; Cassano et al., 2011, 2012; Oddo et al., 2003; Romano et al., 2014). Briefly, brain coronal sections of 20 μm thickness were cut on a cryostat (−20 °C) and thaw-mounted on positively charged slides. Slides were washed with PBS 0.1 M, pH 7.4. The sections were blocked in 5% normal donkey serum/PBS with 0.3% Triton X-100 and then incubated overnight at 4 °C with one of the following antibodies: mouse monoclonal anti-β-amyloid 1–16 (6E10) (1:1000, SIG-39320, Signet Laboratories-Covance, Emeryville, CA, USA), mouse monoclonal anti-tau HT7 (1:1000, MN1000, Thermo Fisher Scientific, Rockford, IL, USA). After washing excess of antibody, sections were developed with a diaminobenzidine substrate using the avidin-biotin horseradish peroxidase system (1:200 dilution, Vector Laboratories). Furthermore, to confirm the background staining level, immunostaining for human APP/Aβ and human tau was also carried out without the primary antibody.

The semi-quantitative analysis of APP/Aβ and tau immunostaining was performed as described in our previous studies (Cassano et al., 2011; Romano et al., 2013, 2014, 2017). In particular, all brain sections were observed under a Nikon Eclipse 80i microscope equipped with a colour charge-coupled device camera and controlled by the software NIS-Elements-BR (Nikon). Slices were photographed in light field at a 4× magnification for the semi-quantitative analyses. The mouse brain atlas (Franklin and Paxinos, 1997) was used as reference for the localization of the brain areas of interest. Aβ- and tau-immunostaining were measured semi-quantitatively as optical density by using the Scion Image software, Image J (Schneider et al., 2012) and considering, for background normalization, the averaged optical density of either non-immunoreactive regions or white matter structures within the same brain slice. The investigator was blind to animal treatment and measurements were obtained in at least three consecutive tissue sections per animal containing the desired structure. Optical densities were calculated as percentage with respect to vehicle-treated 3 × Tg-AD mice, which was set to 100%.

2.11. Quantitative PCR

Total RNA was extracted from brain tissue by TRIzol reagent (Thermo Fisher Scientific, Rockford, IL, USA) according to the following protocol. Isolated RNA was treated with a TURBO DNA-free™ Kit (Thermo Fisher Scientific, Rockford, IL, USA) according to the manufacturer's procedure. cDNA was obtained by reverse transcription of total RNA (2 μg) by using a Maxima H Minus First Strand cDNA Synthesis Kit (Thermo Fisher Scientific, Rockford, IL, USA) according to the manufacturer's procedure. cDNA was used as template for the estimation of human amyloid precursor protein (hAPP) and murine APP (mAPP) gene expression by quantitative PCR (Q-PCR) in a StepOne™ Real-Time PCR System (Applied Biosystems-Thermo Fisher Scientific, Rockford, IL, USA). Reactions were performed in triplicate using SYBR Select Master Mix (Applied Biosystems-Thermo Fisher Scientific, Rockford, IL, USA). Primers were designed using Primer-BLAST software (http://www.ncbi.nlm.nih.gov/tools/primer-blast). The sequences used were the following: hAPP 5′- GATCTCTGAAGTGAATCT GGATGCAG-3′ (forward), 5′- CTAGTTCTGCATCTGCTCAAAG-3′ (reverse); mAPP 5′-TTCGCTGACGGAAACCAAGA-3′ (for), 5′- GAACCTGG TCGAGTGGTCAG-3′ (rev). Glyceraldehyde-3-phosphate dehydrogenase (GAPDH) gene was amplified as endogenous control using the following primers: 5′-TTGCAGTGGCAAAGTGGAGA-3′ (for) and 5′-GTCTCGCTC CTGGAAGATGG-3′ (rev). Data were analysed using the ΔΔCt method. ΔCt was calculated by subtracting the average Ct value of ACTB from the average Ct value of each target gene. ΔΔCt, calculated for each gene, was the difference between the ΔCt of control cells and the ΔCt of treated cells. The relative quantity (RQ) was calculated by $2^{-\Delta\Delta Ct}$.

2.12. Statistical analyses

To determine the pharmacokinetic parameters, the concentration-time data were estimated by a one compartmental method using the R software package version 3.4.0. The C_{max} and t_{max} values were observed with no interpolation. The area under concentration-time curve (AUC) up to the last measured time point ($AUC_{0\rightarrow t}$) was calculated by the trapezoidal rule method. Statistical analysis of pharmacokinetic data were performed by one-way and two-way analyses of variance (ANOVA) followed by Dunnet's *post hoc* multiple comparison method.

Behavioral data were analysed by two-way ANOVA with genotype (3 × Tg-AD *vs* Non-Tg) and mTOR inhibitor treatment (everolimus *vs* vehicle) as between-subject factors. Tukey's honestly significant difference (HSD) test was used for multiple *post hoc* comparisons when required. Biochemical results were analysed by unpaired Student's *t*-test.

Immunohistochemical results were calculated as a percentage of control (vehicle-treated 3 × Tg-AD). The intensity of human APP/Aβ and human tau immunostaining was measured semiquantitatively using their regional optical density. For each animal, measurements were obtained in at least 3 consecutive sections containing the region of interest, for each of these regions, the results were analysed by unpaired Student's t-test. Because of the difference in the number of slides examined, the error degrees of freedom were kept constant at 6 based on the number of animals per group ($n = 4$). The threshold for statistical significance was set at $p < 0.05$. All data were expressed as mean ± SEM.

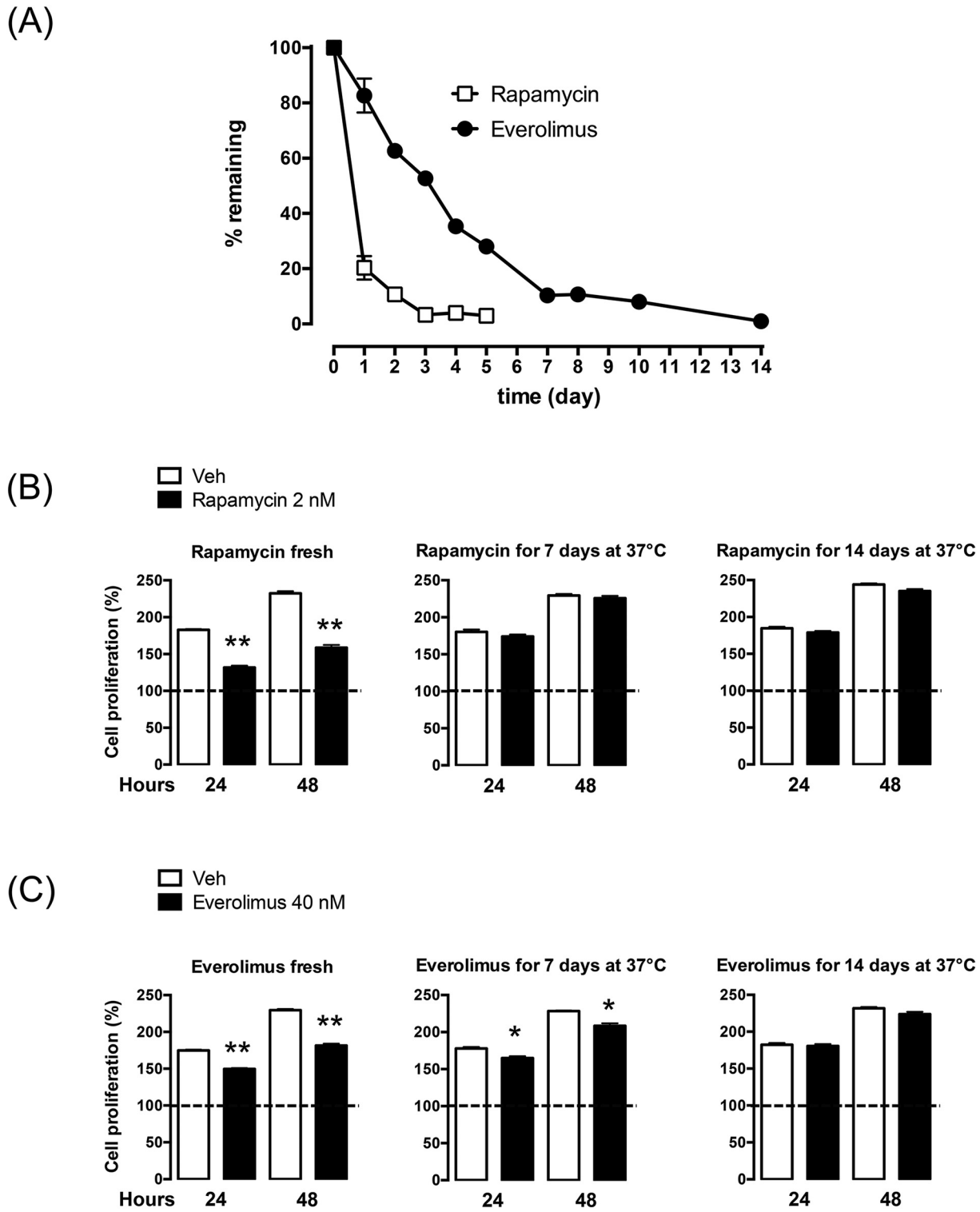

Fig. 1. *Evaluation of everolimus and rapamycin stability in the vehicle solution.* (A) Rapamycin and everolimus (10 μg/ml) were dissolved in DMSO, then diluted in PBS (DMSO 10%) and incubated at 37 °C. The plot of daily HPLC analysis is shown. Stability was determined as percentage of the peak areas at each time point compared with initial values. (B, C) The stability of rapamycin and everolimus was also assessed by the inhibition of SH-SY5Y cell proliferation, measured by MTT method. Cell treatment for 24 and 48 h was performed using both rapamycin (2 nM) and everolimus (40 nM) preparation and normalized to the treatment at 0 h (dashed line). Drugs were solubilized in vehicle (veh) solution, which was used fresh or after incubation at 37 °C for 7 and 14 days. Values are the mean ± SEM (n = 3 per group). Unpaired Student's *t*-test $*p < 0.05$, $**p < 0.01$, rapamycin *vs* vehicle and everolimus *vs* vehicle.

3. Results

3.1. Evaluation of everolimus and rapamycin stability

To determine the stability of the two drugs in suitable conditions for our experimental purposes, rapamycin and everolimus were solubilized in aCSF and aliquots (10 μl) were collected daily for HPLC-UV analysis. As reported in Fig. 1 A, everolimus showed higher stability than its natural analogue at 37 °C, with about 10% of the drug remaining after 10 days of incubation and dropping to zero at day 14, while rapamycin was almost undetectable already by day 4.

To confirm the absence of pharmacological activity in the drug by-products, we also assessed rapamycin and everolimus activity on SH-SY5Y cells. In this experiment, the drugs, solubilized in the same vehicle solution as in the stability experiment, were used fresh or after incubation at 37 °C for 7 and 14 days to simulate the conditions of the drugs within the pumps used for *in vivo* treatment. The dosage used for cell treatment, 2 nM rapamycin and 40 nM everolimus, was established on the basis of their different IC_{50} *vs* mTOR (O'Reilly et al., 2009). As reported in Fig. 1B and C, data indicated that the pharmacological activity at 37 °C completely decays in < 2 weeks, and everolimus showed a longer activity than rapamycin on cell proliferation.

3.2. Pharmacokinetics and mTORC1 inhibition following either single peripheral or central route of administration of everolimus

Pharmacokinetic sampling of everolimus was performed in Non-Tg mice following either a single peripheral (i.p.) or the central (i.c.v.) route of administration. Fig. 2 shows the mean concentration-over-time profiles of everolimus observed in the whole blood (panel A) and in the brain (panel B) after i.p. or i.c.v. administration to different animals.

The blood C_{max} of everolimus was reached at the first sampling time (t_{max} = 1 h), after administration through either route. As expected, both C_{max} and AUC values were considerably higher after i.p. injection as compared to i.c.v. administration. In fact, the latter route produced a blood C_{max} of 94 ± 36 ng/ml with an $AUC_{0\text{-}5h}$ of 269 ± 109 ng h/ml (Fig. 2A); whereas, the i.p. injection produced a blood C_{max} 65 times higher (6149 ± 1064 ng/ml), an estimated nearly 100-fold higher $AUC_{0\text{-}5h}$ (22,736 ± 6005 ng h/ml) and a calculated $t_{1/2}$ of ≈ 4.5 h (Fig. 2A). The results from the i.p. injection matched closely with those previously reported in the literature (O'Reilly et al., 2009).

Despite these differences in the blood, the mean brain C_{max} observed after i.p. or i.c.v. injection of everolimus was identical (255 ± 26 ng/g and 255 ± 15 ng/g, respectively), although it was reached at different sampling time points (1 h and 3 h, respectively, Fig. 2B). The everolimus elimination from the brain ($t_{1/2}$) was apparently slower (≈ 6 h) after i.c.v. administration than from blood (≈ 4.5 h) after i.p. injection.

To estimate everolimus brain permeation through the blood-brain barrier after systemic administration, we calculated the ratio between the brain and the blood concentrations observed at the C_{max} post i.p. administration ($C_{max\text{-}brain}/C_{max\text{-}blood}$ ratio). Thus, we estimated a $C_{max\text{-}brain}/C_{max\text{-}blood}$ ratio of 0.042 (4.2%), suggesting that peripherally administered everolimus enters the brain with low efficiency.

These results suggest that after single peripheral injection everolimus poorly crosses the blood-brain barrier and is slowly metabolized in the brain, due to the longer $t_{1/2}$ of everolimus in the brain compared to blood (6 h *vs* 4.5 h, respectively).

Moreover, the activity of everolimus in the brain after administration through either route was detected by monitoring the phosphorylation of p70S6K. The phosphorylation of p70S6K at threonine 389 has been used as a hallmark of activation by mTOR and has been correlated with the inhibition of autophagy in a number of paradigms. Therefore, the mTORC1 inhibition was detected in mouse brain at equivalent time points of pharmacokinetic after everolimus administration through peripheral or central routes.

Statistical analysis of the immunoblotting revealed a significant main effect of everolimus treatment, regardless of the route of administration (i.p.: $F_{(3,8)} = 49.81$, $p < 0.0001$; i.c.v.: $F_{(3,8)} = 199.6$, $p < 0.0001$) (Fig. 2C–F). Although both peripheral and central routes of administration significantly reduced brain p70S6K threonine phosphorylation at all three sampling time points, the latter induced a much stronger inhibition compared to the former at both 3- and 5-h sampling time points (3 h: – 56% with i.c.v. *vs.* – 30% with i.p.; 5 h: – 41% with i.c.v. *vs.* – 25% with i.p.).

Although the AUC values after i.p. or i.c.v. injection of everolimus were similar ($AUC_{0\text{-}5h}$: 991 ± 119 ng h/ml and 1035 ± 69 ng h/ml, respectively), the brain concentrations of everolimus reached at 3 h and 5 h were higher after i.c.v. administration as compared to i.p. injection (3 h: 255 ± 15 *vs* 210 ± 10, $p = 0.041$, respectively; 5 h: 210 ± 15 *vs* 180 ± 24, n.s., respectively). These data may account for the more pronounced inhibition of mTORC1 inhibition at 3 h and 5 h after i.c.v. infusion. Moreover, the mTOR inhibition in the right (injected) hemisphere might have been even higher compared to the left (non-injected) hemisphere used for the detection.

Therefore, these data suggest that everolimus is more effective in the CNS when administered centrally compared to a peripheral route, although the similar AUC values.

3.3. Effect of everolimus-loaded Alzet pump on mTORC1 inhibition after 3, 5 and 10 days of treatment

The mTORC1 inhibition was evaluated in both brain and liver of Non-Tg mice sub-chronically treated with everolimus (see the timeline of the experiments in Fig. 3). As previously described, everolimus was delivered by a catheter inserted into the lateral ventricle and connected to a subcutaneously implanted osmotic pump (Alzet 1002). Immunoblotting analysis showed a significant reduction of brain p70S6K threonine phosphorylation at 3 (− 45%, $t = 12.25$, df = 4, $p < 0.001$) and 5 (− 15%, $t = 3.020$, df = 4, $p < 0.05$) days from the beginning of treatment, whilst no significant effects were observed at 10 days after intrathecal drug administration when compared with control group (Fig. 4A and B).

To determine the systemic effects of centrally injected everolimus, we evaluated the levels of p70S6K (pT389) in the liver at the same time points as for the brain. Differently from the brain, everolimus did not significantly inhibit mTORC1 in the liver at each time point examined in the analysis, although a trend toward a decrease was observed at 3 days from the beginning of treatment (− 11%, $t = 2.798$, df = 4, n.s.) (Fig. 4C and D).

Moreover, to exclude peripheral effects by i.c.v. everolimus-treatment, we counted the splenocytes and bone marrow cells at 10 days from the beginning of the infusion. Interestingly, the intrathecal infusion of everolimus had no significant effect on the cells from mouse bone marrow and spleen compared to vehicle-treated Non-Tg mice (Supplementary Fig. 1A and B).

3.4. Intrathecal infusion of everolimus reduces the levels of human APP/Aβ and human tau

To determine whether this treatment was effective in slowing down the neuro-functional decline in 3 × Tg-AD mice, a second cohort of mice was intrathecally treated at 6 months of age and sacrificed 1 month later. Their brains were harvested for biochemical and immunohistochemical analyses. In particular, one hemisphere was used for immunohistochemical analysis, whilst the other hemisphere was freshly dissected to isolate hippocampus and frontal cortex, and frozen in dry ice for biochemical analysis. Therefore, we attempted to evaluate whether everolimus treatment modulates the processing of APP and tau phosphorylation in the brain regions mostly affected by the AD-pathology. Western blot analysis of homogenates using 6E10 antibody revealed that everolimus treatment decreased the levels of human full-length APP and Aβ dodecamers, Aβ*56, both in the frontal cortex (−

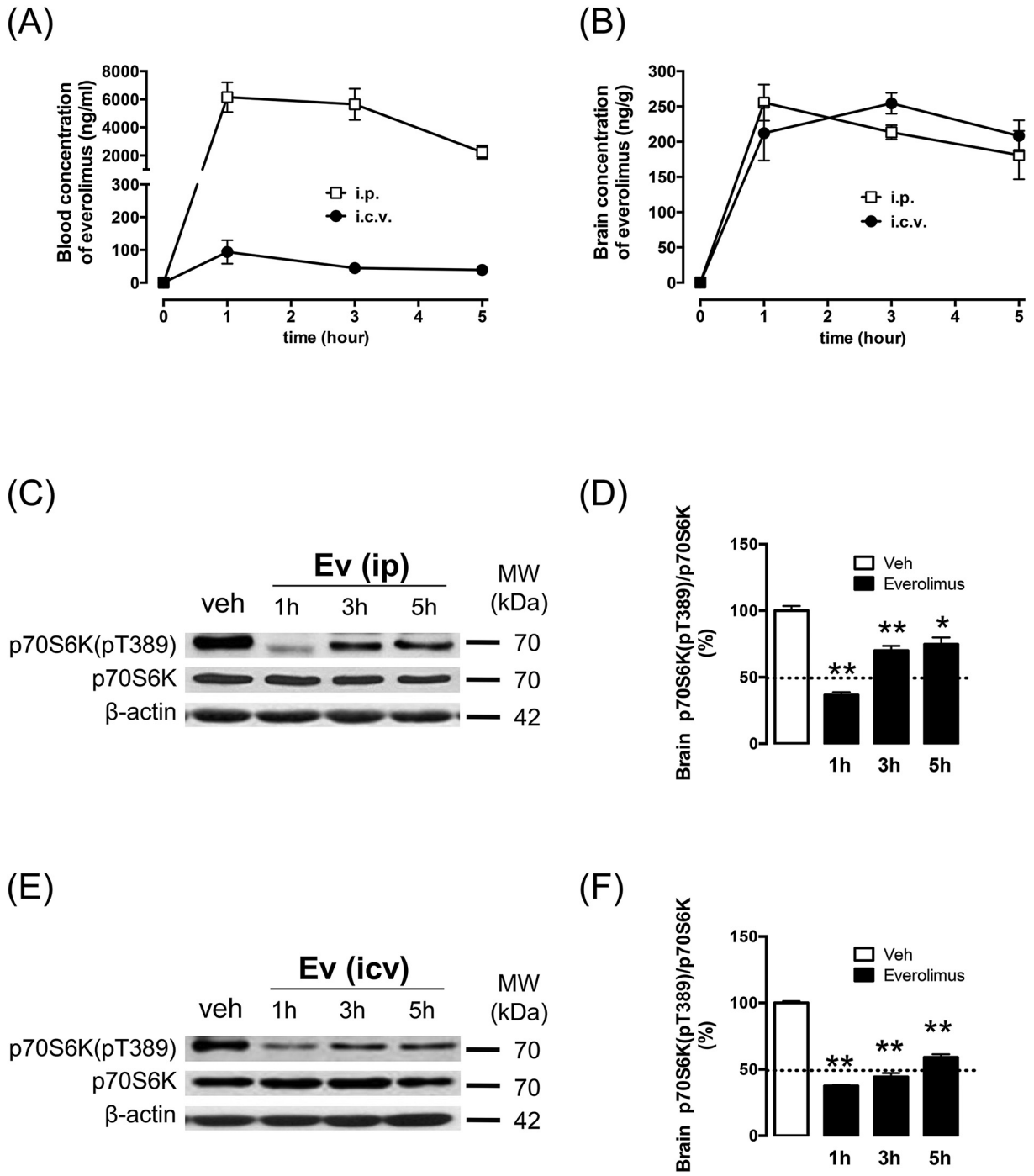

Fig. 2. *Everolimus concentration and mTORC1 signaling after either single intraperitoneal (i.p.) administration or intracerebroventricular (i.c.v.) infusion.* Everolimus-(Ev) was administered as a single peripheral (i.p.) or central (i.c.v.) injection in Non-Tg mice. The whole blood (A) and brain (B) tissue were prepared as described in Methods to perform HPLC-UV analysis. Data are expressed as mean ± SEM (n = 3 per group). Brain proteins were extracted after acute i.p. (C, D) or i.c.v. (E, F) everolimus treatment. Mice were sacrificed after 1, 3 and 5 h to evaluate p70S6K (pT389) by immunoblotting analysis. Data were normalized to total p70S6K expression and expressed as percentage of control. Data are presented as mean ± SEM (n = 3 per group). Unpaired Student's *t*-test *p < 0.05, **p < 0.01, everolimus- *vs* vehicle-treated mice at 1, 3 and 5 h.

37% and – 24%, respectively) (Fig. 5A and B) and in the hippocampus (− 27% and – 26%, respectively) (Fig. 5C and D). The levels of BACE-1, which is involved in APP processing, were unchanged between the vehicle- and everolimus-treated 3 × Tg-AD mice in both brain regions (Fig. 5A–D).

In addition, we found that the levels of tau phosphorylation on residues Ser202/Thr205 (recognized by the AT8 antibody), and Thr231 (AT180 antibody) were not significantly reduced both in the frontal cortex and in the hippocampus, although a trend toward lower AT8 positive tau was observed in everolimus-treated 3 × Tg-AD mice in both brain regions (− 35%, and – 20%, respectively for cortex and hippocampus) (Fig. 5E–H).

Finally, the reduction of Aβ levels was also confirmed by immunohistochemical analysis. At 7 months of age, the 3 × Tg-AD mice typically show widespread intraneuronal Aβ accumulation in a number of brain regions. Immunohistochemical staining revealed an evident

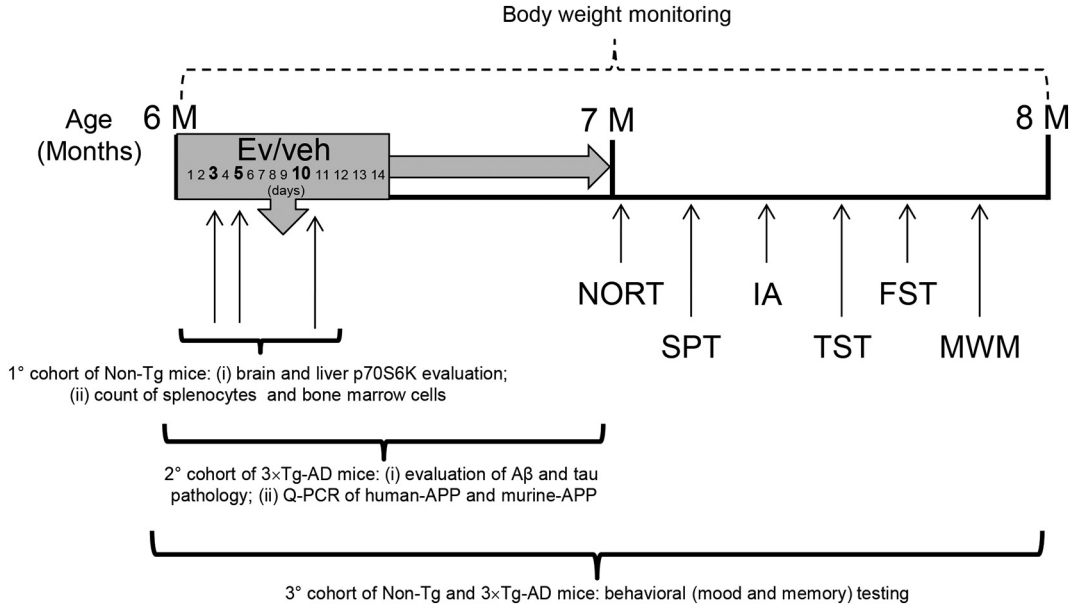

Fig. 3. *Timeline of the experiments performed by osmotic pumps*. A first cohort of 6-month-old Non-Tg mice treated with vehicle (veh) ($n = 9$) or everolimus (Ev) (n = 9) was sacrificed at 3, 5 and 10 days from the beginning of i.c.v. infusion with osmotic pumps. At the end of the treatments, both brains and livers were rapidly excited for western blotting analysis. At 10 days from the beginning of the infusion spleen and femur were also excided and the cells from mouse bone marrow and spleen were counted. A second cohort of 6-month-old 3 × Tg-AD ($n = 5$) mice was injected (i.c.v.) with everolimus (Ev) or vehicle (veh). 4 weeks from the beginning of the treatment, the brains were rapidly excited for the evaluation of Aβ and tau pathology by western blot analysis, immunohistochemistry and Q-PCR. Finally, a third cohort of 6-month-old 3 × Tg-AD ($n = 10$) and Non-Tg (n = 10) mice was injected (i.c.v) with everolimus. Additionally, age- and sex-matched 3 × Tg-AD (n = 10) and Non-Tg (n = 10) mice were treated with vehicle. At the end of the treatment, mice were evaluated in the novel objection recognition test (NORT), tail suspension test (TST), forced swimming test (FST), sucrose preference test (SPT), inhibitory passive avoidance (IA) and Morris water maze (MWM).

contrast in Aβ levels between vehicle- and everolimus-treated 3 × Tg-AD mice in the frontal cortex (Fig. 6A and B) and basolateral amygdala (Fig. 6C and D). Likewise, following everolimus treatment, we observed a marked reduction of intracellular Aβ immunoreactivity in the pyramidal neurons of the hippocampal subiculum, CA1 and CA3 regions (Fig. 6E–N).

To investigate whether everolimus treatment affected tau expression, we have performed other immunohistochemistry experiments designed to analyse the expression patterns of human tau that were recognized by a mouse monoclonal tau antibody (HT7), in a number of brain regions.

We observed an immunoreactive reduction of human tau levels mainly in the frontal cortex and basolateral amygdala (−48% and −45%, respectively) (Fig. 7A–D). Moreover, a significant reduction of human tau immunoreactivity was observed also in the pyramidal neurons of hippocampal CA1 and dorsal CA3 regions (dorsal CA1–23%, ventral CA1–24% and dorsal CA3–21%). Although not significant, we observed a trend toward a decrease (−14%) of HT7 immunostaining in ventral CA3 pyramidal neurons (Fig. 7K and L).

Altogether, these data indicate that early human APP/Aβ and human tau levels in 7-month-old 3 × Tg-AD mice are significantly decreased after brain infusion of everolimus.

3.5. Intrathecal infusion of everolimus did not modify the expression of both hAPP and mAPP genes in the 3 × Tg-AD mice

To exclude that the APP and Abeta56 decrease observed by western blotting is due to the effect of everolimus on the Thy1 promoter, which drives the expression of the hAPP transgenes, the Q-PCR analysis of both human (hAPP) and endogenous murine APP (mAPP) mRNAs was performed from brain tissue of both everolimus- and vehicle-treated mice. As reported in the Supplementary Fig. 3A and B, everolimus treatment did not modify the expression of both hAPP and mAPP genes.

3.6. Intrathecal infusion of everolimus improves learning and memory, and ameliorates the depressive-like phenotype of 3 × Tg-AD mice

We next sought to investigate the effect of everolimus on the behavioral phenotype of 3 × Tg-AD mice, when delivered continuously to the brain by an Alzet pump.

To this aim, at the end of treatment with everolimus 7-month-old 3 × Tg-AD ($n = 10$) and age- and gender-matched Non-Tg mice (n = 10) underwent behavioral tests. As controls, 3 × Tg-AD (n = 10) and Non-Tg mice (n = 10) were treated with vehicle. At this age, the 3 × Tg-AD mice present early learning and memory deficits (Barone et al., 2016; Oddo et al., 2003). We carefully monitored the general health of mice throughout the course of treatment and did not observe any adverse effects or significant changes in their weight gain (data not shown).

To determine the effects of everolimus on learning and memory, 1 month after the beginning of the treatment, mice were tested using three independent behavioral paradigms: the NORT, a behavioral task mainly dependent on multiple cortical areas, the IA, which is highly dependent on the hippocampus and amygdala, and the spatial version of the MWM, a hippocampal-dependent task (Nakazawa et al., 2004; Sutherland and McDonald, 1990). All the statistical analyses from the behavioral tests are reported in Table 1.

The NORT exploits the natural tendency of mice to explore objects perceived as novel. As previously described, the retention session was performed at two different time points (30 min or 24 h) after the exploration session in order to assess both short- and long-term memory, respectively. Two-way ANOVA indicated significant changes in the time mice spent exploring the new object across the four different groups. In particular, at the time point of 30 min (short-term memory), we found significant genotype by treatment interaction effect, while no significant differences were found for the main effect of genotype and treatment. Multiple *post hoc* comparisons showed a significant higher object recognition index for 3 × Tg-AD mice treated with everolimus with respect to vehicle-treated 3 × Tg-AD mice (Fig. 8A and B). When

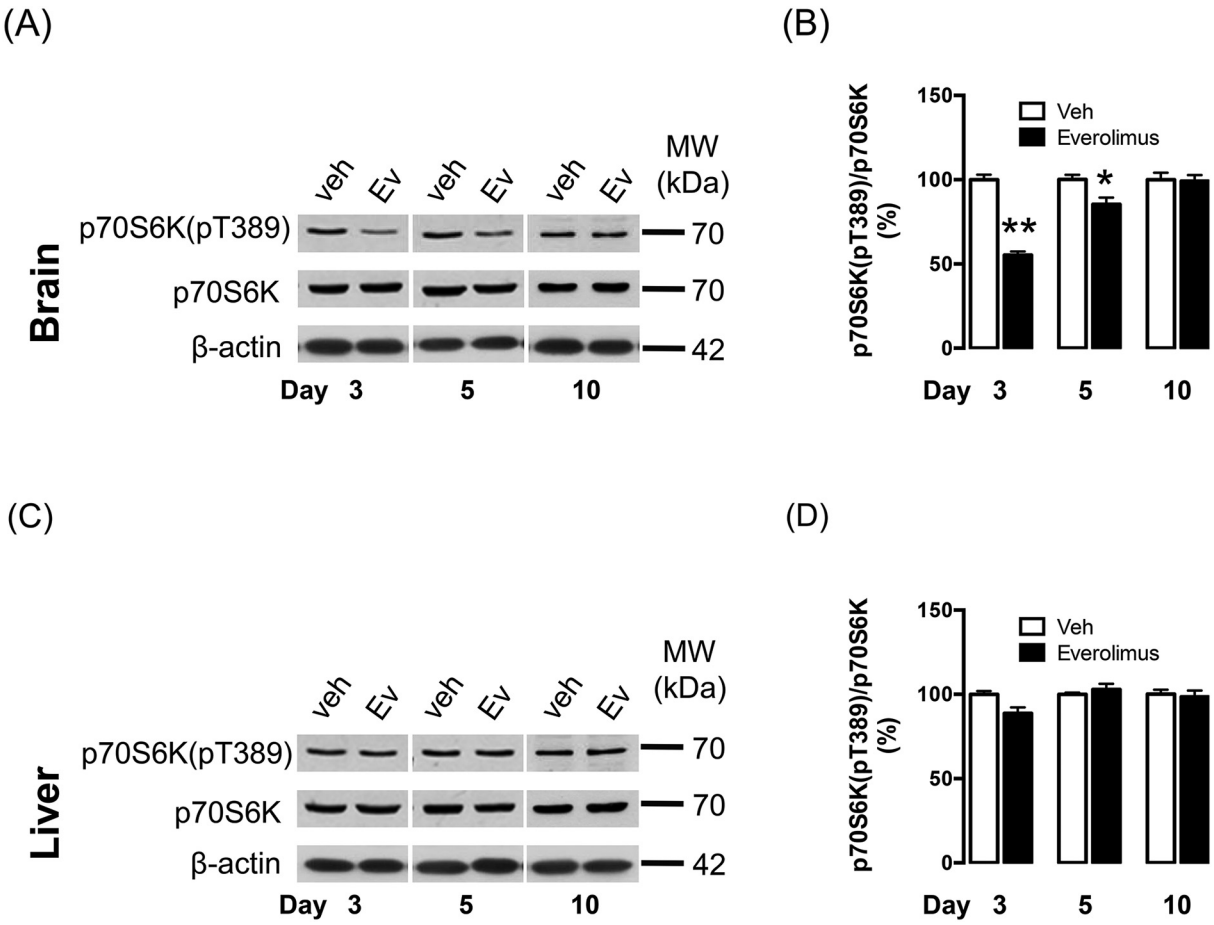

Fig. 4. *Effect of everolimus-loaded Alzet pump on mTORC1 signaling after 3, 5 and 10 days of infusion*. Brain (A, B) and liver (C, D) proteins were extracted from everolimus- (Ev)- or vehicle- (veh)-treated Non-Tg mice sacrificed at 3, 5 and 10 days from the beginning of i.c.v. infusion. Phospho-p70S6K (pT389) was evaluated by immunoblot analysis. Data were normalized to total p70S6K expression and expressed as percentage of control. Data are presented as mean ± SEM (n = 3 per group). Unpaired Student's *t*-test. *p < 0.05, **p < 0.01, everolimus- *vs* vehicle-treated Non-Tg mice.

the probe trial was performed 24 h (long-term memory) later the exploration session, we observed a significant genotype and genotype by treatment interaction effect in the object recognition index among the four groups. The following *post hoc* test showed that everolimus-treated 3 × Tg-AD mice performed significantly better than the vehicle-treated 3 × Tg-AD group (Fig. 8C and D). At both time points, *post hoc* analysis indicated that everolimus had no effect on the performance of Non-Tg mice.

The mice were then evaluated in a contextual learning and memory task (IA), where the retention trials were conducted 24 h or 7 days after the training trial to assess both short- and long-term memory. Statistical analysis indicated at 24 h a significant main effect of genotype and treatment, whilst at 7 days after the training session we observed a significant genotype and genotype by treatment interaction effect. At both time points, the multiple *post hoc* comparisons indicated that everolimus-treated transgenic mice performed at wild-type level and significantly better than 3 × Tg-AD mice treated with vehicle (Fig. 8E). This was not due to differences in sensitivity to the shock, as all mice had similar jump responses upon shock administration.

MWM test mice received 4 training trials per day for 5 days to find the location of a hidden platform. The statistical analysis demonstrated that no significant difference was observed after 5 days of training among the four different groups (escape latencies at day 5 were: Non-Tg/vehicle, 15.7 ± 2; Non-Tg/everolimus, 19.9 ± 2.8; 3 × Tg-AD/vehicle, 14.9 ± 2.9; 3 × Tg-AD/everolimus, 14.9 ± 2.3) (Fig. 8F).

To determine the effects of everolimus on memory, the platform was removed from the maze and probe trials were conducted 1.5 or 24 h following the last training trial to assess both short- and long-term memory, respectively.

When the probe trial was performed at 1.5 or 24 h after the last training session, statistical analysis revealed that everolimus infusion rescued the early memory deficits present in the 3 × Tg-AD mice, as indicated by a significantly decreased latency to cross the platform location of the 3 × Tg-AD mice treated with everolimus compared to vehicle-treated 3 × Tg-AD mice (Fig. 8G and H). Moreover, the time spent in the target quadrant was significantly increased in everolimus-treated 3 × Tg-AD compared to vehicle-treated 3 × Tg-AD mice. Our data were confirmed by the analysis of the swim patterns in the test session. The effects of everolimus on water maze performance were not directly related to motor alterations, since no significant variations of the swimming speed or total distance travelled in the water maze were observed in everolimus compared with vehicle-treated mice (data not shown).

Overall, the 3 × Tg-AD mice treated with everolimus performed similarly to the Non-Tg groups in all probe trials and at both time-points (Fig. 8G and H). Finally, under the conditions used in our study, everolimus had no significant effect on learning or memory retention in the Non-Tg mice (Fig. 8G and H).

Overall, these data indicate that everolimus infusion rescued the early learning and memory deficits in 3 × Tg-AD mice.

Moreover, 3 × Tg-AD and Non-Tg mice treated with either everolimus or vehicle were tested for the depressive-like phenotype in two models of stress-coping behavior (TST and FST) and with an anhedonia test (SPT). All the statistical analyses from the behavioral tests are

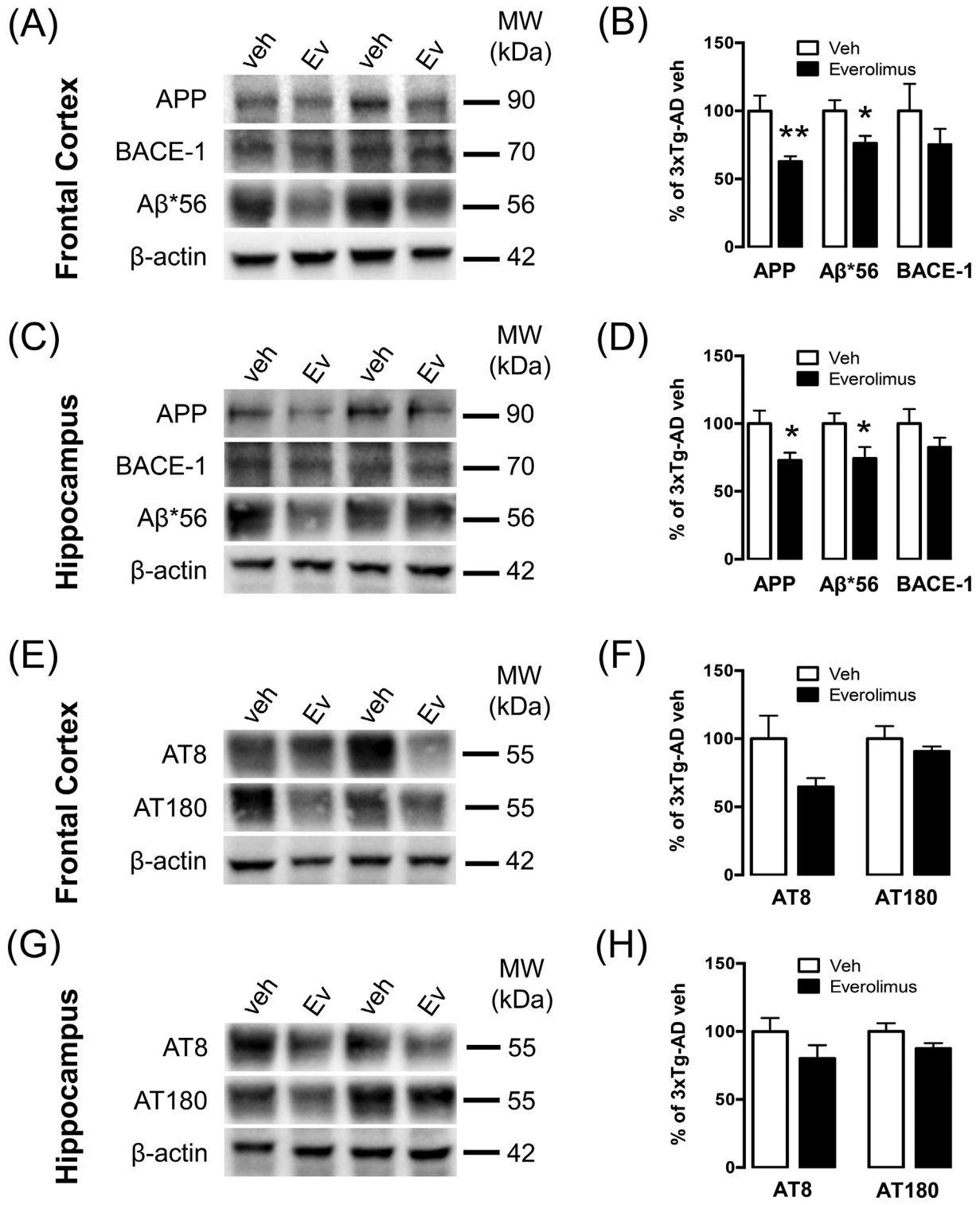

Fig. 5. *Everolimus infusion ameliorates Aβ and tau pathology in the 3 × Tg-AD mice.* Western blot analysis of cortical (A-B) and hippocampal (C-D) homogenates revealed no significant difference in the levels of BACE-1 between vehicle- (veh)- and everolimus- (Ev)- treated 3 × Tg-AD mice. However, the levels of the APP and Aβ dodecamer (Aβ*56) were significantly lower in Ev-treated animals in both frontal cortex (A–B) and hippocampus (C–D). Moreover, a trend toward a decrease of phosphorylated tau levels (AT8 and AT180) were observed in both the frontal cortex (E and F) and hippocampus (G and H) of Ev-treated mice. Data were normalized to β-actin expression and expressed as percentage of vehicle-treated 3 × Tg-AD (n = 5 per group). Data are presented as mean ± SEM and were analysed by unpaired Student's *t*-test. *p < 0.05, **p < 0.01everolimus- *vs* vehicle-treated 3 × Tg-AD mice.

reported in Table 1.

Fig. 8 (I and J) presents the behavioral profile of 3 × Tg-AD and Non-Tg mice in the SPT. As reported in Table 1, we found a significant main effect of genotype, treatment and genotype by treatment interaction. Multiple *post hoc* comparisons showed a significantly increased preference for sucrose in the Non-Tg group compared to the vehicle-treated 3 × Tg-AD mice, and interestingly everolimus restored the preference for the sweet solution in the 3 × Tg-AD group (Fig. 8I).

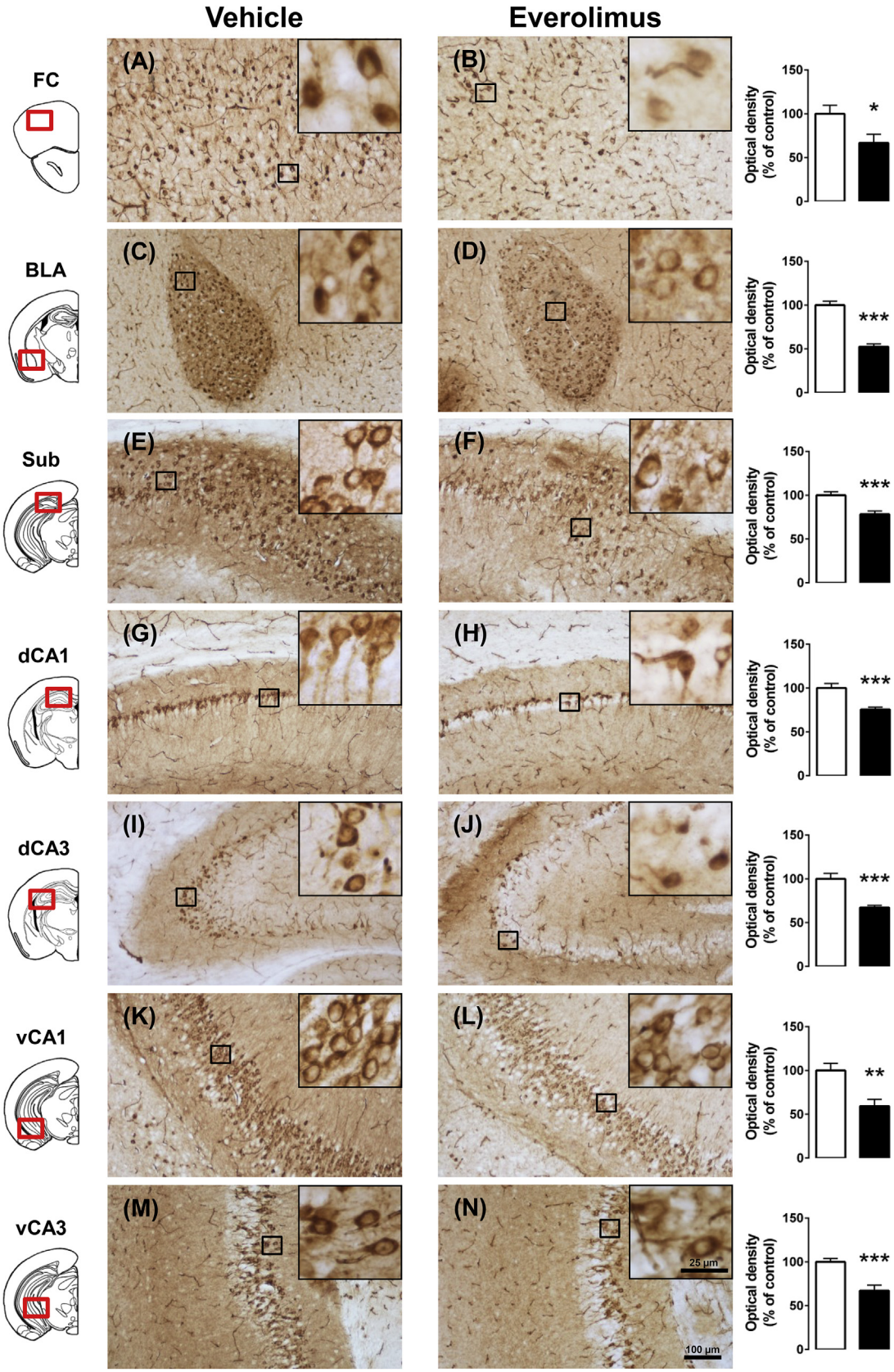

Fig. 6. *Everolimus infusion reduces intracellular human APP/Aβ immunoreactivity*. Representative microphotographs of human APP/Aβ immunostaining (6E10 antibody) from brain coronal sections (20 µm) collected from vehicle- and everolimus-treated 3 × Tg-AD mice. All sections were stained with 3,3′-diaminobenzidine. The inserts show a higher magnification of few neurons. The red squares within the brain diagrams illustrate the sites where the representative microphotographs were taken, whilst the black square within the microphotographs illustrate the sites where the inserts were taken. A – B, frontal cortex (FC); C – D, basolateral amygdala (BLA); E – F, subiculum (Sub); G – H, dorsal CA1 region (dCA1); I – J, dorsal CA3 region (dCA3); K – L, ventral CA1 region (vCA1); M – N, ventral CA3 region (vCA3). Original magnification: 10× for microphotographs, except for the basolateral amygdala captured at 4×; 40× for inserts. Scale bar was set at 100 µm for microphotographs and at 25 µm for inserts.

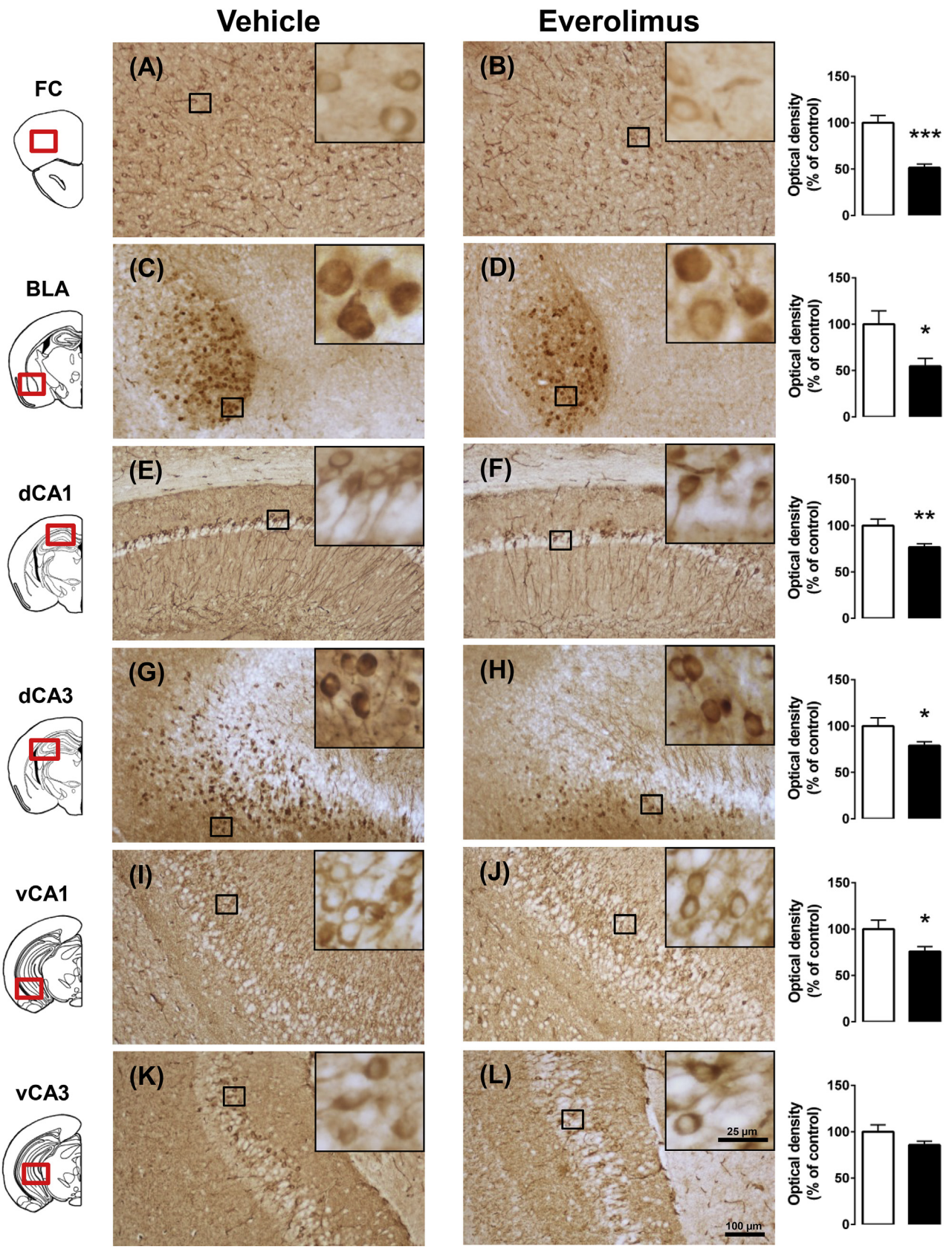

Fig. 7. *Everolimus infusion reduces human tau immunoreactivity*. Representative microphotographs of human tau immunostaining (HT7 antibody) from brain coronal sections (20 µm) collected from vehicle- and everolimus-treated 3 × Tg-AD mice. All sections were stained with 3,3′-diaminobenzidine (DAB). The inserts show a higher magnification of few neurons. The red squares within the brain diagrams illustrate the sites where the representative microphotographs were taken, whilst the black square within the microphotographs illustrate the sites where the inserts were taken. A – B, frontal cortex (FC); C – D, basolateral amygdala (BLA); E – F, dorsal CA1 region (dCA1); G – H, dorsal CA3 region (dCA3); I – J, ventral CA1 region (vCA1); K – L, ventral CA3 region (vCA3). Original magnification 10× for microphotographs, except for the basolateral amygdala captured at 4×; 40× for inserts. Scale bar was set at 100 µm for microphotographs and at 25 µm for inserts.

Table 1
Results from the statistical analysis of data obtained from the behavioral tests.

Behavioral Tests	Parameter	Genotype (G)	Treatment (T)	Interaction (G × T)
NORT	Total exploration time during training (T1)	$F(1,75) = 1.172$, n.s.	$F(1, 75) = 2.044$, n.s.	$F(1, 75) = 0.324$, n.s.
	Total exploration time during testing (T2)	$F(1,75) = 0.170$, n.s.	$F(1, 75) = 0.007$, n.s.	$F(1, 75) = 2.557$, n.s.
	Object recognition index – 30 min	$F(1,37) = 1.916$, n.s.	$F(1,37) = 0.249$, n.s.	$F(1,37) = 7.871$, $p < .01$
	Total exploration time during training (T1)	$F(1,75) = 1.573$, n.s.	$F(1, 75) = 0.0629$, n.s.	$F(1, 75) = 3.884$, n.s.
	Total exploration time during testing (T2)	$F(1,75) = 3.308$, n.s.	$F(1, 75) = 2.764$, n.s.	$F(1, 75) = 0.707$, n.s.
	Object recognition index – 24 h	$F(1,37) = 11.993$, $p < 0.01$	$F(1,37) = 2.617$, n.s.	$F(1,37) = 9.214$, $p < 0.01$
IA	Latency to dark compartment during training	$F(1,34) = 0.580$, n.s.	$F(1,34) = 3.654$, n.s.	$F(1,34) = 0.0179$, n.s.
	Latency to dark compartment – 24 h	$F(1,34) = 11.700$, $p < 0.01$	$F(1,34) = 4.398$, $p < 0.05$	$F(1,34) = 1.077$, n.s.
	Latency to dark compartment during training	$F(1,34) = 1.597$, n.s.	$F(1,34) = 0.071$, n.s.	$F(1,34) = 0.154$, n.s.
	Latency to dark compartment – 7 days	$F(1,34) = 14.017$, $p < 0.001$	$F(1,34) = 0.582$, n.s.	$F(1,34) = 6.855$, $p < 0.05$
MWM	Latency to cross platform location – 1.5 h	$F(1,36) = 19.390$, $p < 0.001$	$F(1,36) = 4.968$, $p < 0.05$	$F(1,36) = 13.069$, $p < 0.001$
	Latency to cross platform location – 24 h	$F(1,36) = 8.409$, $p < .01$	$F(1,36) = 1.270$, n.s.	$F(1,36) = 8.346$, $p < 0.01$
	Time in the target quadrant – 1.5 h	$F(1,36) = 9.468$, $p < 0.01$	$F(1,36) = 2.337$, n.s.	$F(1,36) = 9.231$, $p < 0.01$
	Time in the target quadrant – 24 h	$F(1,36) = 6.186$, $p < 0.05$	$F(1,36) = 3.617$, n.s.	$F(1,36) = 8.199$, $p < 0.01$
TS	Immobility	$F(1,37) = 2.805$, n.s.	$F(1, 37) = 6.846$, $p < 0.05$	$F(1, 37) = 2.537$, n.s.
FS	Immobility	$F(1,37) = 18.975$, $p < 0.001$	$F(1, 37) = 12.549$, $p < 0.01$	$F(1, 37) = 1.999$, n.s.
SPF	Total fluid intake	$F(1,37) = 4.038$, n.s.	$F(1, 37) = 0.620$, n.s.	$F(1, 37) = 0.0832$, n.s.
	Sucrose preference	$F(1,37) = 14.675$, $p < 0.001$	$F(1,37) = 20.972$, $p < 0.001$	$F(1,37) = 44.950$, $p < 0.001$

Two-way analyses of variance (ANOVA) with genotype (3 × Tg-AD *vs* Non-Tg) and mTOR inhibitor treatment (everolimus *vs* vehicle) as between-subject factors. G = genotype, T = treatment. *$p < 0.05$, **$p < 0.01$, ***$p < 0.001$, ($n = 10$ per group). Details are reported in the text.

This effect was not accounted for by a difference in total fluid intake among the four experimental groups (Fig. 8J).

As far as the TST, we found a significant main effect of genotype and treatment but not genotype-by-treatment interaction (Fig. 8K). Subsequent *post hoc* comparisons revealed that the immobility duration was higher in vehicle-treated 3 × Tg-AD mice than in vehicle-treated Non-Tg mice. The infusion of everolimus significantly decreased the immobility duration in the 3 × Tg-AD.

Fig. 8L shows the behavioral profile in the FST comparing differences in immobility time. Two-way ANOVA revealed a significant main effect of treatment and genotype but not genotype-by-treatment interaction. *Post hoc* comparisons showed that immobility time was higher in vehicle-treated 3 × Tg-AD mice than in transgenic mice treated with everolimus and with respect to Non-Tg mice (Fig. 8L).

All together these results suggest that 3 × Tg-AD mice showed an anhedonia-like and a depressive-like and phenotype that was reverted by the everolimus infusion.

4. Discussion

The results of this study demonstrate that a short-term intrathecal infusion of everolimus causes a rapid and long-lasting recovery of cognitive and mood alterations in the early-impaired 3 × Tg-AD mice; moreover, these effects were accompanied by a reduction of human APP/Aβ and human tau levels in a number of cortical regions and limbic areas of the brain.

Everolimus is a rapamycin analog (rapalog) that has been developed to improve the pharmacokinetic characteristics of rapamycin (Lamming et al., 2013). This mTOR inhibitor has been used in immunosuppressive therapy and has been recently evaluated clinically for the treatment of numerous disorders, in particular cancer (Lamming et al., 2013). However, despite mTOR inhibitors having received increasing attention as potential treatments for aging and neurological diseases, no information is available concerning the efficacy of short-term treatments with everolimus in modifying AD-like pathology. Therefore, to our knowledge, this is the first study that explores this potential therapeutic option in a murine model of AD. More interestingly, we proposed in our study to administer everolimus directly into the brain in order to achieve the beneficial effects of mTOR inhibition but with low impact on peripheral organs.

Therefore, the first experiment of our study was designed to compare the *in vitro* stability of everolimus and rapamicyn at body temperature over a long period, which simulates the continuous administration of these mTOR inhibitors when released into the brain through the osmotic pumps. To this aim, we solubilized everolimus in aCSF with a low concentration of DMSO, in order to avoid any possible influence and/or interference with neuronal functioning and the behavioral performance of animals. To this regard, besides the anti-inflammatory and anti-nociceptive properties of DMSO, previous data have already demonstrated that oral and central (i.c.v.) administration of 25% DMSO solution reduces locomotor activity (Colucci et al., 2008). Furthermore, it has been demonstrated the DMSO impairs operant performance in rodents (Castro et al., 1995; Kocsis et al., 1975), an outcome that may have relevant implications in the evaluation of a therapeutic option for AD.

In our experimental paradigms, everolimus was more stable

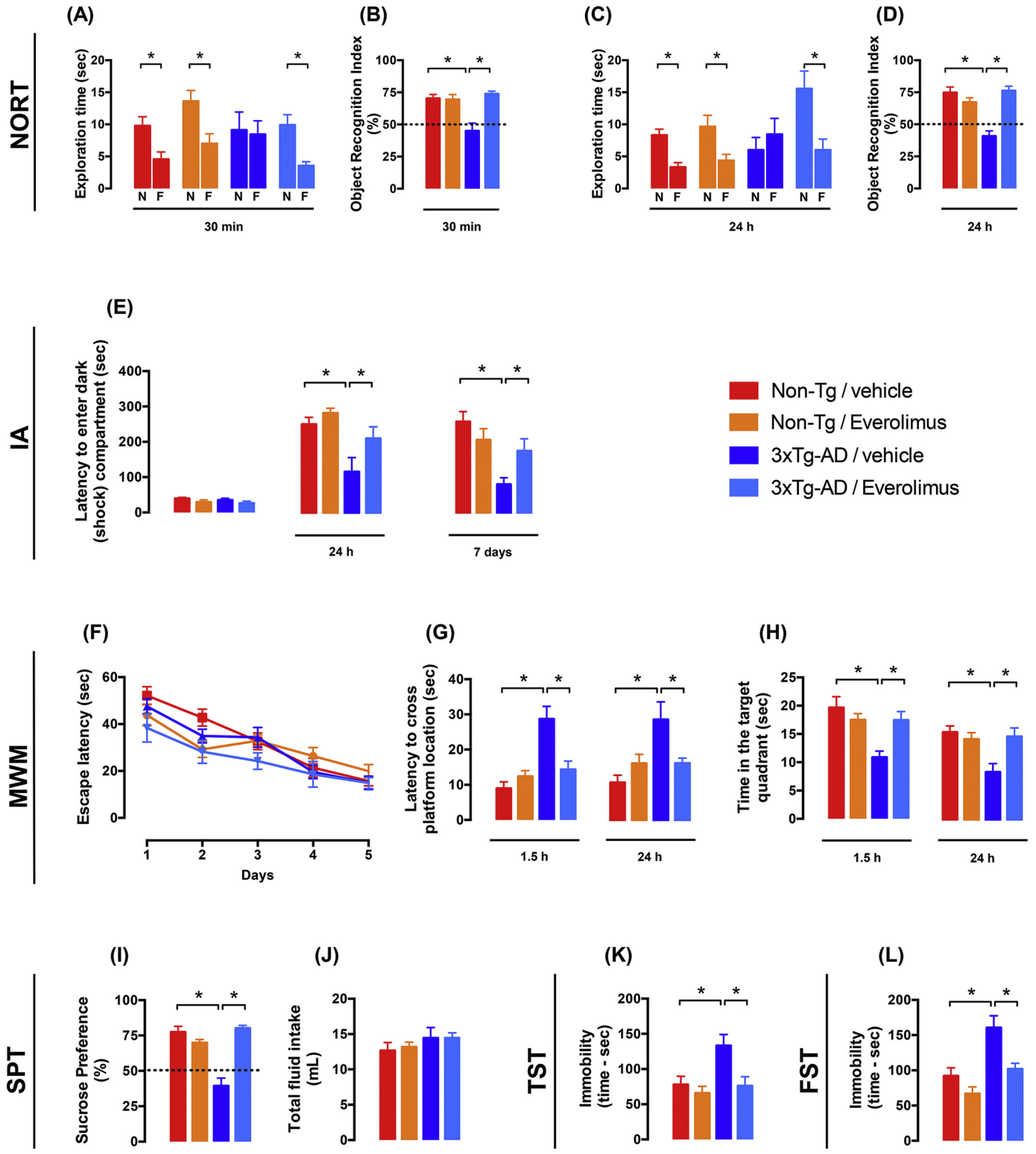

Fig. 8. *Everolimus infusion ameliorates short- and long-term learning and memory, and the depressive-like phenotype in the 3 × Tg-AD mice.* 3 × Tg-AD and Non-Tg mice treated with everolimus or vehicle were evaluated in: (i) novel object recognition test (NORT) (N: novel object; F: familiar object) [A – D, short- (30 min) and long-term (24 h) memory]; (ii) inhibitory passive avoidance (IA) [E, short- (24 h) and long-term (7 days) memory]; (iii) Morris water maze (MWM) [F, escape latency, G and H for short- (1.5 h) and long-term (24 h) memory]; (iv) sucrose preference test (SPT) (I and J); (v) tail suspension test (TST) (K); (vi) forced swimming test (FST) (L). Data are presented as mean ± SEM and were analysed using two-way ANOVA following by *post hoc* Tukey's test to determine individual differences in groups. $^{*}p < 0.05$.

compared to rapamycin. In fact, everolimus concentrations dropped to zero after 14 days of incubation at 37 °C, while rapamycin was almost undetectable after 4 days; moreover, everolimus after incubation for 7 days at 37 °C was still stable enough to significantly inhibit cell proliferation.

Kurdi and colleagues evaluated the effects of short-term (3 days) and long-term (28 days) everolimus administration (1.5 mg/kg/day, subcutaneously) on mTOR inhibition and the induction of autophagy in the liver of mice (Kurdi et al., 2016). The authors used two types of osmotic pumps and dissolved everolimus in a vehicle containing 50% DMSO, reaching an optimal stability of mTOR inhibitor at physiological temperature over an extended time spans (28 days) (Kurdi et al., 2016). In their study, the authors did not investigate the effects of everolimus and vehicle in the brain, but rather focused on the hepatic tissue of treated mice, based on the rationale that the liver is well known to react in a quick and robust manner to the induction of autophagy (Mizushima et al., 2003). The authors reported that the DMSO used as a vehicle in their study had no effect on the observed endpoints (Kurdi et al., 2016); however, on the basis of a large set of data published in the literature, we cannot rule out that a 50% concentration of DMSO might have interfered with our experimental protocol.

More interestingly, Kurdi and colleagues demonstrated that everolimus (1.5 mg/kg/day) fails to inhibit mTOR when administered over long periods (28 days), whilst short-term (3 days) treatment lead to strong mTOR inhibition and a clear stimulation of autophagy (Kurdi et al., 2016). To this regard, many preclinical and clinical studies have previously reported that chronic treatments with rapamycin and its analogs fail to inhibit mTOR signaling (Hassan et al., 2014; Juengel et al., 2012; Wagle et al., 2014). A number of mechanisms have been hypothesized as explanations for the acquired resistance to mTOR inhibitor following their long-term use, including the high phosphorylation status of both Akt1 and S6rp, which are up and downstream regulators of mTOR signaling, respectively (Hassan et al., 2014; Juengel et al., 2012). Likewise, the inhibition of autophagy following long-term everolimus treatment was explained as a consequence of the up-regulation of unc-51 like autophagy activating kinase 1 (ULK1) phosphorylation, that is the main effector through which mTOR initiates autophagy (Kim et al., 2011; Kurdi et al., 2016). Therefore, altogether these data confirm that our intrathecal short-term treatment regimen was appropriate in order to avoid everolimus resistance and to minimize its undesirable immunosuppressive effects.

Orally administered everolimus is considered the treatment of choice for tuberous sclerosis patients, but only in those displaying rapidly growing subependymal giant cells astrocytomas, a life-threatening condition (Krueger et al., 2010). This limitation is caused by the high risk of severe adverse systemic effects linked to the prolonged oral administration of immunosuppressive drugs (Krueger et al., 2010). Moreover, when orally administered in both mice and rats at its efficacious dose, everolimus showed a low gastrointestinal absorption (approximately 12% oral bioavailability), mostly due to its first-pass metabolism both at the intestinal and hepatic level, and more importantly it poorly penetrates the blood-brain barrier (O'Reilly et al., 2009; Yokomasu et al., 2008).

In the light of the above investigations and in accordance with the recommendations of best practice for animal studies in the context of testing novel AD therapies (Shineman et al., 2011), we then evaluated the pharmacokinetics and pharmacodynamics profiles of everolimus following either a single peripheral (i.p.) or central (i.c.v.) route of administration. As expected, our pharmacokinetic study demonstrated that both $c_{max\text{-}blood}$ and AUC_{blood} values resulted in significantly higher values after i.p. injection when compared to i.c.v. infusion. Interestingly, despite the differences in the blood compartment, $c_{max\text{-}brain}$ and AUC_{brain} were similar after both i.p. and i.c.v. injections of everolimus. Moreover, in line with previous published data (O'Reilly et al., 2009), we observed that everolimus poorly crosses the blood-brain barrier and it was eliminated significantly slower from the brain ($t_{1/2\text{-}brain} \approx 6$ h) than from blood ($t_{1/2\text{-}blood} \approx 4.5$ h).

As far as its potential pharmacodynamic profile, we observed that a single intrathecal everolimus infusion decreases the levels of phosphorylated p70S6K in the brain more significantly than an i.p. injection. Moreover, a continuous short-term infusion of everolimus trough osmotic pumps fails to inhibit mTOR signaling in the liver and to reduce the number of splenocytes and bone marrow cells of mice, suggesting that intrathecal infusions are able to increase everolimus brain concentrations while reducing its systemic distribution and associated adverse effects.

These promising results encouraged us to further explore the potential therapeutic effects of intrathecal everolimus administration in a transgenic murine model of AD, which closely mimics the pathology of this disease.

Harrison and colleagues reported the first evidence that feeding rapamycin to mice significantly increased their lifespan (Harrison et al., 2009). One year later, two researchers independently conducted the first studies testing the effects of rapamycin on AD-like pathology in two different AD-transgenic mice (Caccamo et al., 2010; Spilman et al., 2010). In both studies rapamycin was administered at the same dose as that used by Harrison and colleagues (Harrison et al., 2009), and was delivered in the diet to both 6-month-old 3 × Tg-AD mice and 7-month-old hAPP(J20) mice. The authors concluded that rapamycin was able to prevent the initial memory loss in transgenic mice at the earliest stage of AD (Caccamo et al., 2010; Spilman et al., 2010). More interestingly, no effect on memory was observed after a 3-month-treatment with rapamycin in the 3 × Tg-AD mice at 15 months of age, an age at which mice develop widespread plaques and tangles and profound memory deficits (Majumder et al., 2011); differently, 7-month-old hAPP(J20) mice fed with rapamycin for 16 weeks showed no cognitive impairments at 28 months of age (Lin et al., 2013).

Altogether these data suggest that rapamycin is able to rescue memory impairments if administered shortly after the onset of memory deficits but not at later stages of the disease after overt plaque and tangle deposition (Caccamo et al., 2010; Lin et al., 2013; Majumder et al., 2011; Spilman et al., 2010).

Accordingly, here we demonstrate for the first time that a short-term intrathecal everolimus infusion in young/adult 3 × Tg-AD mice rescued cognitive deficits as measured by different behavioral tasks. In particular, in our study a variety of behavioral tests were performed on vehicle- and everolimus-treated mice, including MWM, NORT and IA, which are highly dependent on the hippocampus, cortex and amygdala, brain regions that are affected by AD-pathology. Here, we found no significant difference between vehicle-treated Non-Tg mice and the 3 × Tg-AD mice treated with everolimus, and no detrimental effect of everolimus on memory/cognition in the Non-Tg mice. Thus, at the early stage (7 months of age) of the AD-like pathology we found everolimus-mediated improvements in the short- and long-term memory accompanied by decreased human APP/Aβ and human tau immunoreactivity, which was consistent throughout all hippocampal, cortical, and amygdala areas examined.

In addition to studying the effect of rapamycin and rapalogs on memory, we also demonstrate an emerging role of mTOR inhibition on non-cognitive components of behavior, specifically anxiety- and depressive-like behaviors. In this context, the role of mTOR inhibitors in the modulation of mood disorder is still controversial. For example, Halloran and colleagues have shown that rapamycin reduces depressive-like behaviors, *e.g.*, floating during the training phase of the Morris water maze, and reduced time spent immobile on the tail suspension test (Halloran et al., 2012). Similarly, in a clinical study it has been reported that four weeks everolimus treatment positively affected depression in cardiac transplant patients who had received everolimus as immunosuppressant treatment (Lang et al., 2009). In contrast, other clinical studies did not confirm this effect on renal transplant patients treated with rapamycin (Martínez-Sanchis et al., 2011). In order, to add new insights to this contradictory scenario, the impact of preventive/

therapeutic treatment on non-cognitive symptoms of AD was addressed in the 3 × Tg-AD mice, since they also exhibit a depressive-like phenotype (Romano et al., 2014). Moreover, 3 × Tg-AD mice show a lower basal extracellular output of amines in the frontal cortex and ventral hippocampus and a decreased extracellular response to K^+ stimulation (Romano et al., 2014). Employing a wider range of behavioral tests, our studies demonstrate for the first time that intrathecal everolimus infusion significantly ameliorated the nonmnemonic phenotype of young/adult 3 × Tg-AD mice. In particular, everolimus reverted the depressive-like (tested by FST and TST) and anhedonia-like (tested by SPT) phenotypes of 3 × Tg-AD mice. Although the neuronal mechanisms underlying these effects cannot be explained by our data, we hypothesize that everolimus may increase the monoaminergic tone in 3 × Tg-AD mice. To this regard, it has been demonstrated that the antidepressant-like effects of rapamycin in mice were correlated with increased levels of the three major monoamines (noradrenaline, dopamine and serotonin) and their metabolites in the midbrain (Halloran et al., 2012).

Hence, further investigations are required to better clarify the underlying mechanisms of these everolimus-induced phenotypes in the 3 × Tg-AD mice, which have been revealed in our study for the first time.

5. Conclusions

In summary, our study demonstrates that short-term intrathecal everolimus infusion can reverse the AD-like phenotype observed in the young/adult 3 × Tg-AD mice, *e.g.*, memory is improved and the levels of human APP/Aβ and human tau are reduced. Moreover, our results demonstrate that everolimus has concomitant antidepressant-like effects. This study is consistent with previous studies showing the positive effects of mTOR inhibitors in AD and sheds new light on the short-term intrathecal infusion of everolimus, which is already used in the clinic for different indications. Therefore, the results of the current study may have an important impact for the potential applications in basic and translational research since rapalogs have been approved by the FDA since 1999 and their toxicity profiles are well characterized (Soefje et al., 2011).

Competing interests

The patent WO2013168131 (A1) — 2013-11-14 shares with the present manuscript the authors: Diego Dolcetta, Tommaso Cassano, Alessandro Magini, Stefano Giovagnoli and Carla Emiliani.

Fundings

This research was funded by Dr. Cristina Pigiona (liberal donation), “SMuovilavita” Foundation NPO, “Cuore Livio Mazzonetto” Foundation NPO, “Foundation RSA Agostoni”, “Associazione Ricerca Alzheimer Lissone ARAL” NPO and “Associazione Sclerosi Tuberosa, O.N.L.U.S., Italy (www.sclerosituberosa.org). This project was also supported by the Italian Ministry for Education, University and Research (PRIN20153NBRS3_003 to S.G.) and by Fondazione Terzo Pilastro – Italia e Mediterraneo (Project “ISDIS).

Supplementary data to this article can be found online at https://doi.org/10.1016/j.expneurol.2018.09.011.

Acknowledgements

We thank Dr. Roberto Dominici and Dr. Elisabetta Fortunati for the helpful and critical discussion during manuscript writing.

References

An, W.L., Cowburn, R.F., Li, L., Braak, H., Alafuzoff, I., Iqbal, K., Iqbal, I.G., Winblad, B., Pei, J.J., 2003. Up-regulation of phosphorylated/activated p70 S6 kinase and its relationship to neurofibrillary pathology in Alzheimer's disease. Am. J. Pathol. 163 (2), 591–607. https://doi.org/10.1016/S0002-9440(10)63687-5.

Andrade-Talavera, Y., Benito, I., Casañas, J.J., Rodríguez-Moreno, A., Montesinos, M.L., 2015. Rapamycin restores BDNF-LTP and the persistence of long-term memory in a model of Down's syndrome. Neurobiol. Dis. 82, 516–525. https://doi.org/10.1016/j.nbd.2015.09.005.

Arnell, K., Enblad, P., Wester, T., Sjölin, J., 2007. Treatment of cerebrospinal fluid shunt infections in children using systemic and intraventricular antibiotic therapy in combination with externalization of the ventricular catheter: efficacy in 34 consecutively treated infections. J. Neurosurg. 107 (3 Suppl), 213–219. https://doi.org/10.3171/PED-07/09/213.

Bambico, F.R., Cassano, T., Dominguez-Lopez, S., Katz, N., Walker, C.D., Piomelli, D., Gobbi, G., 2010. Genetic deletion of fatty acid amide hydrolase alters emotional behavior and serotonergic transmission in the dorsal raphe, prefrontal cortex, and hippocampus. Neuropsychopharmacology 35 (10), 2083–2100. https://doi.org/10.1038/npp.2010.80.

Barone, E., Di Domenico, F., Cassano, T., Arena, A., Tramutola, A., Lavecchia, M.A., Coccia, R., Butterfield, D.A., Perluigi, M., 2016. Impairment of biliverdin reductase-A promotes brain insulin resistance in Alzheimer disease: a new paradigm. Free Radic. Biol. Med. 91, 127–142. https://doi.org/10.1016/j.freeradbiomed.2015.12.012.

Barone, E., Tramutola, A., Triani, F., Calcagnini, S., Di Domenico, F., Ripoli, C., Gaetani, S., Grassi, C., Butterfield, D.A., Cassano, T., Perluigi, M., 2018. Biliverdin reductase-A mediates the beneficial effects of intranasal insulin in Alzheimer disease. Mol. Neurobiol. https://doi.org/10.1007/s12035-018-1231-5. (Accepted for publication).

Bedse, G., Romano, A., Cianci, S., Lavecchia, A.M., Lorenzo, P., Elphick, M.R., Laferla, F.M., Vendemiale, G., Grillo, C., Altieri, F., Cassano, T., Gaetani, S., 2014. Altered expression of the CB1 cannabinoid receptor in the triple transgenic mouse model of Alzheimer's disease. J. Alzheimers Dis. 40 (3), 701–712. https://doi.org/10.3233/JAD-131910.

Bellanti, F., Iannelli, G., Blonda, M., Tamborra, R., Villani, R., Romano, A., Calcagnini, S., Mazzoccoli, G., Vinciguerra, M., Gaetani, S., Giudetti, A.M., Vendemiale, G., Cassano, T., Serviddio, G., 2017. Alterations of clock gene RNA expression in brain regions of a triple transgenic model of Alzheimer's disease. J. Alzheimers Dis. 59 (2), 615–631. https://doi.org/10.3233/JAD-160942.

Caccamo, A., Majumder, S., Richardson, A., Strong, R., Oddo, S., 2010. Molecular interplay between mammalian target of rapamycin (mTOR), amyloid-beta, and Tau: effects on cognitive impairments. J. Biol. Chem. 285 (17), 13107–13120. https://doi.org/10.1074/jbc.M110.100420.

Caccamo, A., Maldonado, M.A., Majumder, S., Medina, D.X., Holbein, W., Magrí, A., Oddo, S., 2011. Naturally secreted amyloid-beta increases mammalian target of rapamycin (mTOR) activity via a PRAS40-mediated mechanism. J. Biol. Chem. 286 (11), 8924–8932. https://doi.org/10.1074/jbc.M110.180638.

Cassano, T., Romano, A., Macheda, T., Colangeli, R., Cimmino, C.S., Petrella, A., Laferla, F.M., Cuomo, V., Gaetani, S., 2011. Olfactory memory is impaired in a triple transgenic model of Alzheimer disease. Behav. Brain Res. 224 (2), 408–412. https://doi.org/10.1016/j.bbr.2011.06.029.

Cassano, T., Serviddio, G., Gaetani, S., Romano, A., Dipasquale, P., Cianci, S., Bellanti, F., Laconca, L., Romano, A.D., Padalino, I., Laferla, F.M., Nicoletti, F., Cuomo, V., Vendemiale, G., 2012. Glutamatergic alterations and mitochondrial impairment in a murine model of Alzheimer disease. Neurobiol. Aging 33 (6), 1121.e1–12. https://doi.org/10.1016/j.neurobiolaging.2011.09.021.

Castro, C.A., Hogan, J.B., Benson, K.A., Shehata, C.W., Landauer, M.R., 1995. Behavioral effects of vehicles: DMSO, ethanol, Tween-20, Tween-80, and emulphor-620. Pharmacol. Biochem. Behav. 50 (4), 521–526.

Chen, G., Chen, K.S., Knox, J., Inglis, J., Bernard, A., Martin, S.J., Justice, A., McConlogue, L., Games, D., Freedman, S.B., Morris, R.G., 2000. A learning deficit related to age and beta-amyloid plaques in a mouse model of Alzheimer's disease. Nature 408 (6815), 975–979. https://doi.org/10.1038/35050103.

Colucci, M., Maione, F., Bonito, M.C., Piscopo, A., Di Giannuario, A., Pieretti, S., 2008. New insights of dimethyl sulphoxide effects (DMSO) on experimental in vivo models of nociception and inflammation. Pharmacol. Res. 57 (6), 419–425. https://doi.org/10.1016/j.phrs.2008.04.004.

Ehninger, D., Han, S., Shilyansky, C., Zhou, Y., Li, W., Kwiatkowski, D.J., Ramesh, V., Silva, A.J., 2008. Reversal of learning deficits in a Tsc2+/− mouse model of tuberous sclerosis. Nat. Med. 14 (8), 843–848. https://doi.org/10.1038/nm1788.

Fraenkel, M., Ketzinel-Gilad, M., Ariav, Y., Pappo, O., Karaca, M., Castel, J., Berthault, M.F., Magnan, C., Cerasi, E., Kaiser, N., Leibowitz, G., 2008. mTOR inhibition by rapamycin prevents beta-cell adaptation to hyperglycemia and exacerbates the metabolic state in type 2 diabetes. Diabetes 57 (4), 945–957. https://doi.org/10.2337/db07-0922.

Franklin, K.B.J., Paxinos, G., 1997. The Mouse Brain in Stereotaxic Coordinates. Academic Press, San Diego, CA.

Fried, H.I., Nathan, B.R., Rowe, A.S., Zabramski, J.M., Andaluz, N., Bhimraj, A., Guanci, M.M., Seder, D.B., Singh, J.M., 2016. The Insertion and Management of External Ventricular Drains: an Evidence-Based Consensus Statement: a Statement for Healthcare Professionals from the Neurocritical Care Society. Neurocrit. Care. 24 (1), 61–81. https://doi.org/10.1007/s12028-015-0224-8.

Giovagnoli, S., Cassano, T., Pace, L., Magini, A., Polchi, A., Tancini, B., Perluigi, M., De Marco, F., Emiliani, C., Dolcetta, D., 2015. Evaluation of a LC-MS method for everolimus preclinical determination in brain by using [(13)C2D4]RAD001 internal standard. J. Chromatogr. B Analyt. Technol. Biomed. Life Sci. 985, 155–163. https://doi.org/10.1016/j.jchromb.2015.01.035.

Giustino, A., Cagiano, R., Carratù, M.R., Cassano, T., Tattoli, M., Cuomo, V., 1999. Prenatal exposure to low concentrations of carbon monoxide alters habituation and non-spatial working memory in rat offspring. Brain Res. 844 (1–2), 201–205. https://doi.org/10.1038/sj.bjp.0702143.

Halloran, J., Hussong, S.A., Burbank, R., Podlutskaya, N., Fischer, K.E., Sloane, L.B., Austad, S.N., Strong, R., Richardson, A., Hart, M.J., Galvan, V., 2012. Chronic inhibition of mammalian target of rapamycin by rapamycin modulates cognitive and

non-cognitive components of behavior throughout lifespan in mice. Neuroscience 223, 102–113. https://doi.org/10.1016/j.neuroscience.2012.06.054.
Harrison, D.E., Strong, R., Sharp, Z.D., Nelson, J.F., Astle, C.M., Flurkey, K., Nadon, N.L., Wilkinson, J.E., Frenkel, K., Carter, C.S., Pahor, M., Javors, M.A., Fernandez, E., Miller, R.A., 2009. Rapamycin fed late in life extends lifespan in genetically heterogeneous mice. Nature 460 (7253), 392–395. https://doi.org/10.1038/nature08221.
Hassan, B., Akcakanat, A., Sangai, T., Evans, K.W., Adkins, F., Eterovic, A.K., Zhao, H., Chen, K., Chen, H., Do, K.A., Xie, S.M., Holder, A.M., Naing, A., Mills, G.B., Meric-Bernstam, F., 2014. Catalytic mTOR inhibitors can overcome intrinsic and acquired resistance to allosteric mTOR inhibitors. Oncotarget 5 (18), 8544–8557. https://doi.org/10.18632/oncotarget.2337.
Iyer, A.M., van Scheppingen, J., Milenkovic, I., Anink, J.J., Adle-Biassette, H., Kovacs, G.G., Aronica, E., 2014. mTOR Hyperactivation in down syndrome hippocampus appears early during development. J. Neuropathol. Exp. Neurol. 73 (7), 671–683. https://doi.org/10.1097/NEN.0000000000000083.
Juengel, E., Dauselt, A., Makarević, J., Wiesner, C., Tsaur, I., Bartsch, G., Haferkamp, A., Blaheta, R.A., 2012. Acetylation of histone H3 prevents resistance development caused by chronic mTOR inhibition in renal cell carcinoma cells. Cancer Lett. 324 (1), 83–90. https://doi.org/10.1016/j.canlet.2012.05.003.
Katz, R.J., 1982. Animal model of depression: pharmacological sensitivity of a hedonic deficit. Pharmacol. Biochem. Behav. 16 (6), 965–968.
Kim, J., Kundu, M., Viollet, B., Guan, K.L., 2011. AMPK and mTOR regulate autophagy through direct phosphorylation of Ulk1. Nat. Cell Biol. 13 (2), 132–141. https://doi.org/10.1038/ncb2152.
Kocsis, J.J., Harkaway, S., Snyder, R., 1975. Biological effects of the metabolites of dimethyl sulfoxide. Ann. N. Y. Acad. Sci. 243, 104–109.
Korfel, A., Schlegel, U., 2013. Diagnosis and treatment of primary CNS lymphoma. Nat. Rev. Neurol. 9 (6), 317–327. https://doi.org/10.1038/nrneurol.2013.83.
Krueger, D.A., Care, M.M., Holland, K., Agricola, K., Tudor, C., Mangeshkar, P., Wilson, K.A., Byars, A., Sahmoud, T., Franz, D.N., 2010. Everolimus for subependymal giant-cell astrocytomas in tuberous sclerosis. N. Engl. J. Med. 363 (19), 1801–1811. https://doi.org/10.1056/NEJMoa1001671.
Kurdi, A., De Doncker, M., Leloup, A., Neels, H., Timmermans, J.P., Lemmens, K., Apers, S., De Meyer, G.R.Y., Martinet, W., 2016. Continuous administration of the mTORC1 inhibitor everolimus induces tolerance and decreases autophagy in mice. Br. J. Pharmacol. 173 (23), 3359–3371. https://doi.org/10.1111/bph.13626.
Lamming, D.W., Ye, L., Sabatini, D.M., Baur, J.A., 2013. Rapalogs and mTOR inhibitors as anti-aging therapeutics. J. Clin. Invest. 123 (3), 980–989. https://doi.org/10.1172/JCI64099.
Lang, U.E., Heger, J., Willbring, M., Domula, M., Matschke, K., Tugtekin, S.M., 2009. Immunosuppression using the mammalian target of rapamycin (mTOR) inhibitor everolimus: pilot study shows significant cognitive and affective improvement. Transplant. Proc. 41 (10), 4285–4288. https://doi.org/10.1016/j.transproceed.2009.08.050.
Lin, A.L., Zheng, W., Halloran, J.J., Burbank, R.R., Hussong, S.A., Hart, M.J., Javors, M., Shih, Y.Y., Muir, E., Solano Fonseca, R., Strong, R., Richardson, A.G., Lechleiter, J.D., Fox, P.T., Galvan, V., 2013. Chronic rapamycin restores brain vascular integrity and function through NO synthase activation and improves memory in symptomatic mice modeling Alzheimer's disease. J. Cereb. Blood Flow Metab. 33 (9), 1412–1421. https://doi.org/10.1038/jcbfm.2013.82.
Lin, A.L., Jahrling, J.B., Zhang, W., Derosa, N., Bakshi, V., Romero, P., Galvan, V., Richardson, A., 2017. Rapamycin rescues vascular, metabolic and learning deficits in apolipoprotein E4 transgenic mice with pre-symptomatic Alzheimer's disease. J. Cereb. Blood Flow Metab. 37 (1), 217–226. https://doi.org/10.1177/0271678X15621575.
Mabuchi, S., Altomare, D.A., Cheung, M., Zhang, L., Poulikakos, P.I., Hensley, H.H., Schilder, R.J., Ozols, R.F., Testa, J.R., 2007. RAD001 inhibits human ovarian cancer cell proliferation, enhances cisplatin-induced apoptosis, and prolongs survival in an ovarian cancer model. Clin. Cancer Res. 13 (14), 4261–4270. https://doi.org/10.1158/1078-0432.CCR-06-2770.
Magini, A., Polchi, A., Di Meo, D., Mariucci, G., Sagini, K., De Marco, F., Cassano, T., Giovagnoli, S., Dolcetta, D., Emiliani, C., 2017. TFEB activation restores migration ability to Tsc1-deficient adult neural stem/progenitor cells. Hum. Mol. Genet. 26 (17), 3303–3312. https://doi.org/10.1093/hmg/ddx214.
Majumder, S., Richardson, A., Strong, R., Oddo, S., 2011. Inducing autophagy by rapamycin before, but not after, the formation of plaques and tangles ameliorates cognitive deficits. PLoS One 6 (9), e25416. https://doi.org/10.1371/journal.pone.0025416.
Majumder, S., Caccamo, A., Medina, D.X., Benavides, A.D., Javors, M.A., Kraig, E., Strong, R., Richardson, A., Oddo, S., 2012. Lifelong rapamycin administration ameliorates age-dependent cognitive deficits by reducing IL-1β and enhancing NMDA signaling. Aging Cell 11 (2), 326–335. https://doi.org/10.1111/j.1474-9726.2011.00791.x.
Martínez-Sanchis, S., Bernal, M.C., Montagud, J.V., Candela, G., Crespo, J., Sancho, A., Pallardó, L.M., 2011. Effects of immunosuppressive drugs on the cognitive functioning of renal transplant recipients: a pilot study. J. Clin. Exp. Neuropsychol. 33 (9), 1016–1024. https://doi.org/10.1080/13803395.2011.595396.
Mizushima, N., Yamamoto, A., Matsui, M., Yoshimori, T., Ohsumi, Y., 2003. In vivo analysis of autophagy in response to nutrient starvation using transgenic mice expressing a fluorescent autophagosome marker. Mol. Biol. Cell 15 (3), 1101–1111. https://doi.org/10.1091/mbc.E03-09-0704.
Motzer, R.J., Escudier, B., Oudard, S., Hutson, T.E., Porta, C., Bracarda, S., Grünwald, V., Thompson, J.A., Figlin, R.A., Hollaender, N., Urbanowitz, G., Berg, W.J., Kay, A., Lebwohl, D., Ravaud, A., 2008. RECORD-1 Study Group. Efficacy of everolimus in advanced renal cell carcinoma: a double-blind, randomised, placebo-controlled phase III trial. Lancet 372 (9637), 449–456. https://doi.org/10.1016/S0140-6736(08)61039-9.
Muller, M.A., Beutner, F., Teupser, D., Ceglarek, U., Thiery, J., 2008. Prevention of atherosclerosis by the mtor inhibitor everolimus in ldlr−/− mice despite severe hypercholesterolemia. Atherosclerosis 198, 39–48. https://doi.org/10.1016/j.atherosclerosis.2007.09.019.
Nakazawa, K., McHugh, T.J., Wilson, M.A., Tonegawa, S., 2004. NMDA receptors, place cells and hippocampal spatial memory. Nat. Rev. Neurosci. 5 (5), 361–372. https://doi.org/10.1038/nrn1385.
Oddo, S., Caccamo, A., Shepherd, J.D., Murphy, M.P., Golde, T.E., Kayed, R., Metherate, R., Mattson, M.P., Akbari, Y., Laferla, F.M., 2003. Triple-transgenic model of Alzheimer's disease with plaques and tangles: intracellular Abeta and synaptic dysfunction. Neuron 39 (3), 409–421. https://doi.org/10.1016/S0896-6273(03)00434-3.
O'Reilly, T., McSheehy, P.M., Kawai, R., Kretz, O., McMahon, L., Brueggen, J., Bruelisauer, A., Gschwind, H.P., Allegrini, P.R., Lane, H.A., 2009. Comparative pharmacokinetics of RAD001 (everolimus) in normal and tumor-bearing rodents. Cancer Chemother. Pharmacol. 65 (4), 625–639. https://doi.org/10.1007/s00280-009-1068-8.
Peyrl, A., Chocholous, M., Azizi, A.A., Czech, T., Dorfer, C., Mitteregger, D., Gojo, J., Minichmayr, E., Slavc, I., 2014. Safety of Ommaya reservoirs in children with brain tumors: a 20-year experience with 5472 intraventricular drug administrations in 98 patients. J. Neuro-Oncol. 120 (1), 139–145. https://doi.org/10.1007/s11060-014-1531-1.
Polchi, A., Magini, A., Mazuryk, J., Tancini, B., Gapiński, J., Patkowski, A., Giovagnoli, S., Emiliani, C., 2016. Rapamycin loaded solid lipid nanoparticles as a new tool to deliver mTOR inhibitors: formulation and in vitro characterization. Nano 6 (5), 87. https://doi.org/10.3390/nano6050087.
Porsolt, R.D., Lepichon, M., Jalfre, M., 1977. Depression - new animal model sensitive to antidepressant treatments. Nature 266, 730–732.
Powers, R.W. 3rd, Kaeberlein, M., Caldwell, S.D., Kennedy, B.K., Fields, S., 2006. Extension of chronological life span in yeast by decreased TOR pathway signaling. Genes Dev. 20(2): 174–84. doi: https://doi.org/10.1101/gad.1381406.
Romano, A., Cassano, T., Tempesta, B., Cianci, S., Dipasquale, P., Coccurello, R., Cuomo, V., Gaetani, S., 2013. The satiety signal oleoylethanolamide stimulates oxytocin neurosecretion from rat hypothalamic neurons. Peptides 49, 21–26. https://doi.org/10.1016/j.peptides.2013.08.006.
Romano, A., Pace, L., Tempesta, B., Lavecchia, A.M., Macheda, T., Bedse, G., Petrella, A., Cifani, C., Serviddio, G., Vendemiale, G., Gaetani, S., Cassano, T., 2014. Depressive-like behavior is paired to monoaminergic alteration in a murine model of Alzheimer's disease. Int. J. Neuropsychopharmacol. 18(4). pii: pyu020. doi: https://doi.org/10.1093/ijnp/pyu020.
Romano, A., Gallelli, C.A., Koczwara, J.B., Braegger, F.E., Vitalone, A., Falchi, M., Micioni Di Bonaventura, M.V., Cifani, C., Cassano, T., Lutz, T.A., Gaetani, S., 2017. Role of the area postrema in the hypophagic effects of oleoylethanolamide. Pharmacol. Res. 122, 20–34. https://doi.org/10.1016/j.phrs.2017.05.017.
Schneider, C.A., Rasband, W.S., Eliceiri, K.W., 2012. NIH image to ImageJ: 25 years of image analysis. Nat. Methods 9 (7), 671–675. https://doi.org/10.1038/nmeth.2089.
Scuderi, C., Bronzuoli, M.R., Facchinetti, R., Pace, L., Ferraro, L., Broad, K.D., Serviddio, G., Bellanti, F., Palombelli, G., Carpinelli, G., Canese, R., Gaetani, S., Steardo, L. Jr, Steardo, L., Cassano, T., 2018. Ultramicronized palmitoylethanolamide rescues learning and memory impairments in a triple transgenic mouse model of Alzheimer's disease by exerting anti-inflammatory and neuroprotective effects. Transl. Psychiatry 8(1): 32. doi: https://doi.org/10.1038/s41398-017-0076-4.
Shineman, D.W., Basi, G.S., Bizon, J.L., Colton, C.A., Greenberg, B.D., Hollister, B.A., Lincecum, J., Leblanc, G.G., Lee, L.B., Luo, F., Morgan, D., Morse, I., Refolo, L.M., Riddell, D.R., Scearce-Levie, K., Sweeney, P., Yrjänheikki, J., Fillit, H.M., 2011. Accelerating drug discovery for Alzheimer's disease: best practices for preclinical animal studies. Alzheimers Res. Ther. 3 (5), 28. https://doi.org/10.1186/alzrt90.
Soefje, S.A., Karnad, A., Brenner, A.J., 2011. Common toxicities of mammalian target of rapamycin inhibitors. Target. Oncol. 6 (2), 125–129. https://doi.org/10.1007/s11523-011-0174-9.
Spilman, P., Podlutskaya, N., Hart, M.J., Debnath, J., Gorostiza, O., Bredesen, D., Richardson, A., Strong, R., Galvan, V., 2010. Inhibition of mTOR by rapamycin abolishes cognitive deficits and reduces amyloid-beta levels in a mouse model of Alzheimer's disease. PLoS One 5 (4), e9979. https://doi.org/10.1371/journal.pone.0009979.
Stallone, G., Infante, B., Pontrelli, P., Ranieri, E., Loverre, A., Schena, A., Cormio, L., Carrieri, G., Schena, F.P., Grandaliano, G., Gesualdo, L., 2009. ID2-VEGF-related pathways in the pathogenesis of Kaposi's sarcoma: a link disrupted by rapamycin. Am. J. Transplant. 9 (3), 558–566. https://doi.org/10.1111/j.1600-6143.2008.02537.x.
Sutherland, R.J., McDonald, R.J., 1990. Hippocampus, amygdala, and memory deficits in rats. Behav. Brain Res. 37 (1), 57–79.
Vellai, T., Takacs-Vellai, K., Zhang, Y., Kovacs, A.L., Orosz, L., Müller, F., 2003. Genetics: influence of TOR kinase on lifespan in C. elegans. Nature 426 (6967), 620. https://doi.org/10.1038/426620a.
Wagle, N., Grabiner, B.C., Van Allen, E.M., Amin-Mansour, A., Taylor-Weiner, A., Rosenberg, M., Gray, N., Barletta, J.A., Guo, Y., Swanson, S.J., Ruan, D.T., Hanna, G.J., Haddad, R.I., Getz, G., Kwiatkowski, D.J., Carter, S.L., Sabatini, D.M., Jänne, P.A., Garraway, L.A., Lorch, J.H., 2014. Response and acquired resistance to everolimus in anaplastic thyroid cancer. N. Engl. J. Med. 371 (15), 1426–1433. https://doi.org/10.1056/NEJMoa1403352.
Yokomasu, A., Yano, I., Sato, E., Masuda, S., Katsura, T., Inui, K., 2008. Effect of intestinal and hepatic first-pass extraction on the pharmacokinetics of everolimus in rats. Drug Metab. Pharmacokinet. 23 (6), 469–475. https://doi.org/10.2133/dmpk.23.469.